3540 *Inorg. Chem.* **2010**, *49*, 3540–3552
DOI: 10.1021/ic100104t

Inorganic Chemistry
Article

Fourth Generation Scorpionates: Coordination Behavior of a New Class of Conformationally Flexible Mixed-Donor (Pyrazol-1-yl)borates

Elena V. Mutseneck, Susanne Bieller, Michael Bolte, Hans-Wolfram Lerner, and Matthias Wagner*

Institut für Anorganische und Analytische Chemie, Goethe-Universität Frankfurt, Max-von-Laue-Strasse 7, D-60438 Frankfurt (Main), Germany

Received January 18, 2010

The coordination behavior, the conformational flexibility, and the stability of the novel (pyrazol-1-yl)borate ligands $[Ph(pz)B(\mu\text{-}N(Me))(\mu\text{-}pz)B(pz)Ph]^-$ ($[\mathbf{L^1}]^-$), $[Ph(pz)B(\mu\text{-}O)(\mu\text{-}pz)B(pz)Ph]^-$ ($[\mathbf{L^2}]^-$), and $[Ph(pz)B(\mu\text{-}O)(\mu\text{-}OB(Ph)O)B(pz)Ph]^{2-}$ ($[\mathbf{L^3}]^{2-}$) have been experimentally assessed by investigating the following compounds: $[Li(thf)\mathbf{L^1}]$, $[Li(thf)\mathbf{L^2}]$, $[Mg(Cl)(thf)_x\mathbf{L^1}]$, $[Mg(Cl)(thf)_2\mathbf{L^2}]$, $[Mn(CO)_3\mathbf{L^2}]$, $K(thf)[Mn(CO)_3\mathbf{L^3}]$, $[CoCl_2(H\mathbf{L^1})]$, $[\mathbf{L^1}Co(\mu\text{-}Cl)_2Co\mathbf{L^1}]$, $[Zn(Br)\mathbf{L^1}]$, $[Cu(Cl)\mathbf{L^1}]$, $[Cu(Cl)\mathbf{L^2}]$. The $\mathbf{L^1}$-complexes were prepared from a mixture of $H\mathbf{L^1}$ and the appropriate metal salt by addition of a base. HCl elimination from $[CoCl_2(H\mathbf{L^1})]$, which gives $[\mathbf{L^1}Co(\mu\text{-}Cl)_2Co\mathbf{L^1}]$, does not necessarily require the assistance of a base, but happens spontaneously when a solution of the complex is stored at room temperature for several days. $K(thf)[Mn(CO)_3\mathbf{L^3}]$ was obtained via in situ hydrolysis of $H\mathbf{L^1}/[Mn(CO)_5Br]$ in the presence of K_2CO_3. In some other cases, formation of the coordination compounds proceeded with decomposition of a part of the ligand molecules and yielded pyrazole (e.g., $[Zn(Cl)(Hpz)\mathbf{L^2}]$) or pyrazolide (e.g., $[\mathbf{L^2}Co(\mu\text{-}Cl)(\mu\text{-}pz)Co\mathbf{L^2}]$) complexes. As evidenced by the crystal structure analyses of $[Zn(Br)\mathbf{L^1}]/[Mg(Cl)(thf)_2\mathbf{L^2}]/[Mn(CO)_3\mathbf{L^2}]$ on the one hand and $[\mathbf{L^1}Mg(\mu\text{-}Cl)_2Mg(thf)\mathbf{L^1}]/[Cu(Cl)\mathbf{L^1}]/[Cu(Cl)\mathbf{L^2}]_2$ on the other, $[\mathbf{L^1}]^-$ and $[\mathbf{L^2}]^-$ are able to adopt both a facial and a meridional conformation. Moreover, while many of the established design principles of scorpionate chemistry are still valid for $[\mathbf{L^1}]^-$, $[\mathbf{L^2}]^-$, and $[\mathbf{L^3}]^{2-}$, the bonding situation of the central donor moiety (N(Me) in $[\mathbf{L^1}]^-$; O in $[\mathbf{L^2}]^-$, $[\mathbf{L^3}]^{2-}$) is distinctly different from the way the pyrazolyl rings are attached to the molecule, so that donor scrambling is not an issue in these [*N,N,N*] and [*N,O,N*] mixed-donor ligands.

Introduction

Poly(pyrazol-1-yl)borates ("scorpionates") of the general formula $[R'R''B(^Rpz)_2]^-$ are extremely versatile ligands with applications ranging from cluster chemistry, bioinorganic chemistry, and homogeneous catalysis to materials sciences (^Rpz = (substituted) pyrazol-1-yl; R′, R″ = H, alkyl, aryl, ^Rpz).[1,2]

Already the first generation of scorpionates, which consisted merely of species $[H_2B(^Rpz)_2]^-$, $[HB(^Rpz)_3]^-$, and $[^RpzB(^Rpz)_3]^-$ bearing pyrazol-1-yl or 3,5-dimethylpyrazol-1-yl donor groups, enjoyed tremendous interest because of their relationship to the highly popular β-diketonate and cyclopentadienyl ligands. However, because the coordination chemistry of first generation scorpionates is dominated by the formation of unreactive ML_2 (instead of ML(X)) complexes,[3] the application range of the new ligand class in homogeneous catalysis soon turned out to be limited.

Thus, to stabilize ML(X)-type complexes and to be able to influence the ligands' cone and wedge angles, "second generation scorpionates" with bulky substituents (e.g., Ph, *t*Bu) on the 3-positions of their pyrazolyl rings have been developed and are nowadays widely used.[3]

Finally, the term "third generation scorpionates" was coined to designate poly(pyrazol-1-yl)borates (and methanes) that are specifically functionalized at the non-coordinating, "back" position.[4] Such modifications can help, for example, to influence the crystal packing of scorpionate complexes and thereby to bring about cooperative solid-state behavior,[4] or to create oligotopic scorpionate ligands as scaffolds for oligonuclear metal complexes.[5−20]

A further extension of the scope of scorpionate ligands requires (i) control not only over their steric demand but also

*To whom correspondence should be addressed. E-mail: matthias.wagner@chemie.uni-frankfurt.de.

(1) Trofimenko, S. *Scorpionates - The Coordination Chemistry of Polypyrazolylborate Ligands*; Imperial College Press: London, 1999.
(2) Pettinari, C. *Scorpionates II: Chelating Borate Ligands*; Imperial College Press: London, 2008.
(3) Trofimenko, S.; Calabrese, J. C.; Thompson, J. S. *Inorg. Chem.* **1987**, *26*, 1507–1514.
(4) Reger, D. L.; Gardinier, J. R.; Gemmill, W. R.; Smith, M. D.; Shahin, A. M.; Long, G. J.; Rebbouh, L.; Grandjean, F. *J. Am. Chem. Soc.* **2005**, *127*, 2303–2316.
(5) Fabrizi de Biani, F.; Jäkle, F.; Spiegler, M.; Wagner, M.; Zanello, P. *Inorg. Chem.* **1997**, *36*, 2103–2111.
(6) Guo, S. L.; Peters, F.; Fabrizi de Biani, F.; Bats, J. W.; Herdtweck, E.; Zanello, P.; Wagner, M. *Inorg. Chem.* **2001**, *40*, 4928–4936.
(7) Bieller, S.; Zhang, F.; Bolte, M.; Bats, J. W.; Lerner, H.-W.; Wagner, M. *Organometallics* **2004**, *23*, 2107–2113.

Published on Web 03/03/2010

over their ligand field strength and (ii) the design of conformationally more flexible frameworks that are able to support meridional in addition to the common facial coordination modes.

The first problem has already been tackled by various research groups who developed, "non-pyrazolyl scorpionates" $[R'B(Do)_3]^-$ possessing functional groups Do with donor atoms other than N (e.g., P,[21,22] S[23−28]). For a systematic tuning of metal complex properties, it is, however, desirable to possess complete homogeneous series of closely related ligands of the form $[R'B(Do^1)_x(Do^2)_{3-x}]^-$ (x = 0 to 3). Unfortunately, this is where scorpionate chemistry exhibits its weaknesses because (i) the selective preparation of a specific mixed-donor borate is often difficult to achieve, and (ii) borate ions have a tendency for substituent scrambling.

At this point, we became interested in the question how the architecture of classic poly(pyrazol-1-yl)borates can be modified further to meet current challenges of homogeneous catalysis. Compounds of the type $\mathbf{HL^1}/[\mathbf{L^1}]^-$ and $[Li(thf)\mathbf{L^2}]$ (Figure 1) appeared to be particularly attractive, because they present a mixed-donor set to the metal ion, and the bite angle between the two pyrazolyl moieties should be sufficiently large to make meridional binding a realistic option.

The purpose of this paper is to explore the coordination behavior, the conformational flexibility, and the stability of $\mathbf{HL^1}/[\mathbf{L^1}]^-$ and $[Li(thf)\mathbf{L^2}]$, for which we suggest the name, "fourth generation scorpionates".

Results and Discussion

Both compounds, $\mathbf{HL^1}$ and $[Li(thf)\mathbf{L^2}]$ (Figure 1), have already been described in the literature.[29,30] $\mathbf{HL^1}$ is accessible via

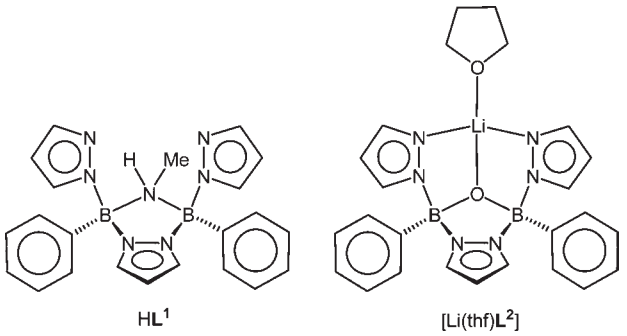

Figure 1. Two fourth generation scorpionates: $\mathbf{HL^1}$ and $[Li(thf)\mathbf{L^2}]$.

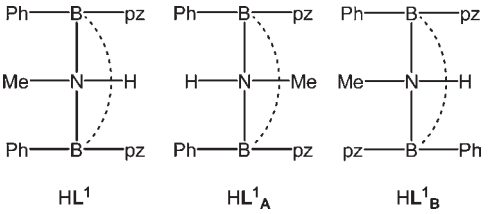

Figure 2. Three experimentally observed isomers $\mathbf{HL^1}$, $\mathbf{HL^1_A}$, and $\mathbf{HL^1_B}$.

the reaction of (i) the borazine derivative $(B(Ph)N(Me))_3$ with Hpz (1:3) in refluxing hexane or (ii) the diborylamine derivative $(Me_2N(Ph)B)_2NMe$ with Hpz (1:2.85) in refluxing Et_2O.

We preferred the second route, which gives higher yields; however, we modified the published synthesis protocol[29] in the following way: (i) The key compound $(Me_2N(Ph)B)_2$-NMe was prepared from $Me_2N(Ph)BBr$[31,32] (instead of $Me_2N(Ph)BCl$) and $(Me_3Si)_2NMe$ (pentane, −78 °C).[33] (ii) The reaction time in the final step of synthesis sequence was reduced from 25 to 12 h.

As already reported,[29] the crude product of the synthesis of $\mathbf{HL^1}$ consists of a mixture of three isomers ($\mathbf{HL^1}$, $\mathbf{HL^1_A}$, and $\mathbf{HL^1_B}$; Figure 2) in a stoichiometric ratio of approximately 8:1:2. After recrystallization from hexane/benzene, only the more abundant mirror-symmetric isomer $\mathbf{HL^1}$ was left, together with $\mathbf{HL^1_B}$ (approximate ratio = 4:1; ^{1}H NMR spectroscopic control).

The X-ray crystal structure analysis of $\mathbf{HL^1}$ (Figure 3; Table 1) revealed that the methyl group of the bridging N(H)-Me moiety points toward the two phenyl rings, whereas the H-atom is obviously engaged in intramolecular hydrogen bonds with the pyrazolyl substituents (N(1)···N(12) = 2.850(4) Å, N(1)···N(22) = 2.825(4) Å; N(1)−H(1)−N(12) = 121(2)°, N(1)−H(1)−N(22) = 119(2)°). We assume this bifurcated hydrogen bond to be one reason why isomer $\mathbf{HL^1}$ is formed in higher amount than $\mathbf{HL^1_A}$ and $\mathbf{HL^1_B}$. This view is consistent with the fact, that the synthesis of $[Li(thf)\mathbf{L^2}]$ does not suffer from isomer formation, most likely because of a structure-directing template effect of the Li^+ ion.

(8) Zhang, F.; Bolte, M.; Lerner, H.-W.; Wagner, M. *Organometallics* **2004**, *23*, 5075–5080.
(9) Bieller, S.; Bolte, M.; Lerner, H.-W.; Wagner, M. *Inorg. Chem.* **2005**, *44*, 9489–9496.
(10) Haghiri Ilkhechi, A.; Mercero, J. M.; Silanes, I.; Bolte, M.; Scheibitz, M.; Lerner, H.-W.; Ugalde, J. M.; Wagner, M. *J. Am. Chem. Soc.* **2005**, *127*, 10656–10666.
(11) Reger, D. L.; Watson, R. P.; Smith, M. D.; Pellechia, P. J. *Organometallics* **2005**, *24*, 1544–1555.
(12) Casado, M. A.; Hack, V.; Camerano, J. A.; Ciriano, M. A.; Tejel, C.; Oro, L. A. *Inorg. Chem.* **2005**, *44*, 9122–9124.
(13) Reger, D. L.; Watson, R. P.; Smith, M. D. *Inorg. Chem.* **2006**, *45*, 10077–10087.
(14) Reger, D. L.; Watson, R. P.; Gardinier, J. R.; Smith, M. D.; Pellechia, P. J. *Inorg. Chem.* **2006**, *45*, 10088–10097.
(15) Reger, D. L.; Watson, R. P.; Smith, M. D.; Pellechia, P. J. *Organometallics* **2006**, *25*, 743–755.
(16) Zhang, F.; Morawitz, T.; Bieller, S.; Bolte, M.; Lerner, H.-W.; Wagner, M. *Dalton Trans.* **2007**, 4594–4598.
(17) Ruth, K.; Tüllmann, S.; Vitze, H.; Bolte, M.; Lerner, H.-W.; Holthausen, M. C.; Wagner, M. *Chem.—Eur. J.* **2008**, *14*, 6754–6770.
(18) Morawitz, T.; Zhang, F.; Bolte, M.; Bats, J. W.; Lerner, H.-W.; Wagner, M. *Organometallics* **2008**, *27*, 5067–5074.
(19) Qin, Y.; Cui, C.; Jäkle, F. *Macromolecules* **2008**, *41*, 2972–2974.
(20) Reger, D. L.; Foley, E. A.; Watson, R. P.; Pellechia, P. J.; Smith, M. D.; Grandjean, F.; Long, G. J. *Inorg. Chem.* **2009**, *48*, 10658–10669.
(21) Barney, A. A.; Heyduk, A. F.; Nocera, D. G. *Chem. Commun.* **1999**, 2379–2380.
(22) Betley, T. A.; Peters, J. C. *Inorg. Chem.* **2003**, *42*, 5074–5084.
(23) Ge, P.; Haggerty, B. S.; Rheingold, A. L.; Riordan, C. G. *J. Am. Chem. Soc.* **1994**, *116*, 8406–8407.
(24) Ohrenberg, C.; Ge, P.; Schebler, P.; Riordan, C. G.; Yap, G. P. A.; Rheingold, A. L. *Inorg. Chem.* **1996**, *35*, 749–754.
(25) Ohrenberg, C.; Riordan, C. G.; Liable-Sands, L.; Rheingold, A. L. *Coord. Chem. Rev.* **1998**, *174*, 301–311.
(26) Schebler, P. J.; Riordan, C. G.; Guzei, I. A.; Rheingold, A. L. *Inorg. Chem.* **1998**, *37*, 4754–4755.
(27) Kimblin, C.; Bridgewater, B. M.; Hascall, T.; Parkin, G. *J. Chem. Soc., Dalton Trans.* **2000**, 1267–1274.
(28) Ibrahim, M. M.; Seebacher, J.; Steinfeld, G.; Vahrenkamp, H. *Inorg. Chem.* **2005**, *44*, 8531–8538.
(29) Bielawski, J.; Das, M. K.; Hanecker, E.; Niedenzu, K.; Nöth, H. *Inorg. Chem.* **1986**, *25*, 4623–4628.
(30) Bieller, S.; Bolte, M.; Lerner, H.-W.; Wagner, M. *Chem.—Eur. J.* **2006**, *12*, 4735–4742.
(31) Barfield, P. A.; Lappert, M. F.; Lee, J. *J. Chem. Soc. A* **1968**, 554–559.
(32) Brown, C.; Cragg, R. H.; Miller, T. J.; Smith, D. O. *J. Organomet. Chem.* **1983**, *244*, 209–215.
(33) To obtain decent yields (60−65%), it is essential to strictly maintain a stoichiometric ratio $Me_2N(Ph)BBr/(Me_3Si)_2NMe$ of 2:1 and to use carefully dried $(Me_3Si)_2NMe$.

Somewhat surprisingly, the B−N bonds to the four-coordinate central nitrogen atom are only slightly longer than those to the sp^2-hybridized nitrogen atoms of the bridging pyrazolyl ring (av. values: 1.600(4) Å vs 1.586(4) Å). For the B−N bonds to the dangling pyrazolyl substituents, however, we find significantly shorter lengths (av. value: 1.542(4) Å). This observation indicates that the pyrazolide backbone might be slightly too short to create a strain-free ligand framework.

Main Group Metal Complexes of $[L^1]^-$ and $[L^2]^-$: [Li(thf)L^1], [Mg(Cl)(thf)$_x L^1$], and [Mg(Cl)(thf)$_2 L^2$]. Treatment of HL^1 in tetrahydrofuran (THF, thf) with 1 equiv of *n*-BuLi in hexane at −78 °C gives [Li(thf)L^1] in essentially quantitative yield (Scheme 1). The analogous reaction with MeMgCl in THF resulted in the formation of the corresponding magnesium complex [Mg(Cl)(thf)$_x L^1$] (Scheme 1), which is extremely sensitive to air and moisture. Interestingly, [Mg(Cl)(thf)$_x L^1$] cannot be prepared from [Li(thf)L^1] by salt metathesis, since the addition of anhydrous $MgCl_2$ to a solution of the lithium compound in THF (stoichiometric ratio = 1:1) causes decomposition of the (pyrazol-1-yl)borate ligand (^{1}H NMR spectroscopic control). In contrast, we were able to synthesize [Mg(Cl)(thf)$_2 L^2$] from the [*N*,*O*,*N*] ligand [Li(thf)L^2] and $MgCl_2$ in 88% yield (Scheme 1).

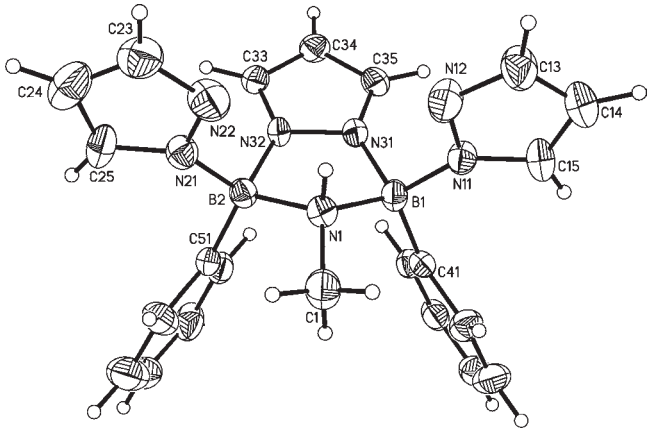

Figure 3. Molecular structure of HL^1. Displacement ellipsoids are drawn at the 50% probability level. Selected bond lengths [Å], atom···atom distances [Å], angles [deg], and dihedral angles [deg]: B(1)−N(1) 1.599(4), B(1)−N(11) 1.539(4), B(1)−N(31) 1.583(4), B(2)−N(1) 1.601(4), B(2)−N(21) 1.545(4), B(2)−N(32) 1.589(4), N(1)−C(1) 1.493(4), N(1)···N(12) 2.850(4), N(1)···N(22) 2.825(4); B(1)−N(1)−B(2) 110.5(2), N(1)−B(1)−N(31) 96.9(2), N(1)−B(2)−N(32) 96.6(2), C(1)−N(1)−B(1) 116.5(2), C(1)−N(1)−B(2) 115.6(2), N(1)−H(1)−N(12) 121(2), N(1)−H(1)−N(22) 119(2); N(1)B(1)B(2)//B(1)B(2)N(31)N(32) 31.5.

Even though the samples of HL^1 used in these syntheses were mixtures of two isomers (HL^1 and HL^1_B), the NMR spectra of [Li(thf)L^1] and [Mg(Cl)(thf)$_x L^1$] did not show resonances attributable to (deprotonated) HL^1_B. Given the reproducibly high yields, we come to the conclusion that the contaminant has not simply been removed in the recrystallization step. We rather assume that deprotonation of HL^1_B induces a rearrangement of the molecular framework, because now the central N(Me) fragment can act as π-electron donor toward the boron atoms and thereby facilitate the dissociation of a terminal pyrazolyl ring. In the subsequent reassociation step, the template

Scheme 1. Synthesis of [Li(thf)L^1], [Mg(Cl)(thf)$_x L^1$], and [Mg(Cl)(thf)$_2 L^2$][a]

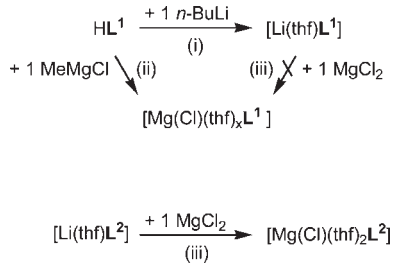

[a] (i) THF/hexane, −78 °C; (ii) THF, −78 °C; (iii) THF, r.t. (room temperature).

Table 1. Selected Crystallographic Data of HL^1, [Li(thf)L^1], and [L^1Mg(μ-Cl)$_2$Mg(thf)L^1]

compound	HL^1	[Li(thf)L^1]	[L^1Mg(μ-Cl)$_2$Mg(thf)L^1]·C_5H_{12}
formula	$C_{22}H_{23}B_2N_7$	$C_{26}H_{30}B_2LiN_7O$	$C_{53}H_{64}B_4Cl_2Mg_2N_{14}O$
fw	407.09	485.13	1075.94
color, shape	colorless, block	colorless, block	colorless, block
temperature (K)	173(2)	173(2)	173(2)
crystal system	monoclinic	monoclinic	triclinic
space group	$P2_1/n$	$P2_1$	$P\bar{1}$
a (Å)	9.8415(12)	10.1477(6)	10.3916(5)
b (Å)	12.8740(10)	19.4929(12)	11.3166(7)
c (Å)	16.9876(18)	14.3962(8)	25.0748(14)
α (deg)	90	90	80.102(4)
β (deg)	94.607(9)	109.867(4)	79.144(4)
γ (deg)	90	90	80.988(4)
V (Å^3)	2145.4(4)	2678.2(3)	2829.2(3)
Z	4	4	2
$D_{calcd.}$ (g cm^{-3})	1.260	1.203	1.263
F(000)	856	1024	1132
μ (mm^{-1})	0.078	0.075	0.189
crystal size (mm^3)	0.24 × 0.23 × 0.14	0.30 × 0.30 × 0.16	0.32 × 0.30 × 0.27
no. of rflns collected	17392	36111	36341
no. of indep rflns (R_{int})	3784 (0.1104)	5210 (0.0721)	10976 (0.0423)
data/restraints/parameters	3784/0/285	5210/1/667	10976/37/685
GOF on F^2	0.964	1.026	1.031
*R*1, *wR*2 ($I > 2\sigma(I)$)	0.0589, 0.1127	0.0452, 0.1093	0.0508, 0.1435
*R*1, *wR*2 (all data)	0.1173, 0.1311	0.0548, 0.1141	0.0584, 0.1496
largest diff peak and hole (e Å^{-3})	0.337, −0.209	0.338, −0.326	0.888, −0.721

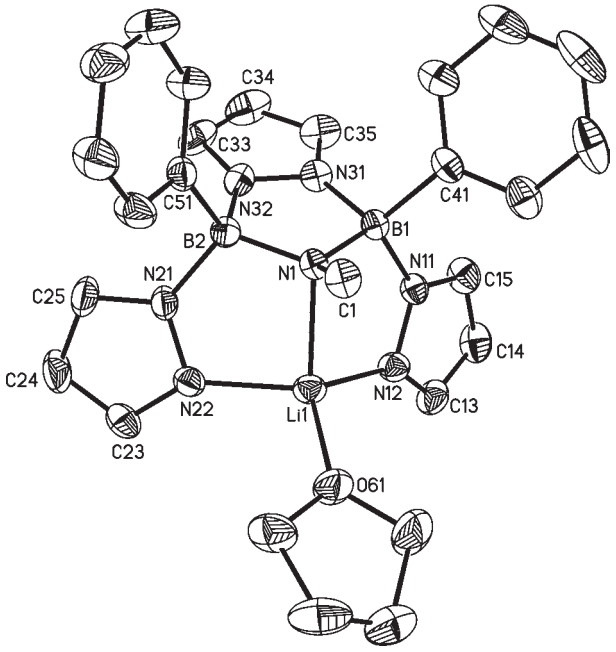

Figure 4. Molecular structure of [Li(thf)$\mathbf{L^1}$]. The H-atoms are omitted for clarity; displacement ellipsoids are drawn at the 50% probability level. Selected bond lengths [Å], angles [deg], and dihedral angles [deg]: Li(1)−N(1) 2.093(6), Li(1)−N(12) 2.015(6), Li(1)−N(22) 1.993(6), Li(1)−O(61) 1.923(5), B(1)−N(1) 1.530(4), B(1)−N(11) 1.593(4), B(1)−N(31) 1.587(4), B(2)−N(1) 1.528(4), B(2)−N(21) 1.574(4), B(2)−N(32) 1.589(4), N(1)−C(1) 1.465(4); N(1)−Li(1)−N(12) 89.7(2), N(1)−Li(1)−N(22) 90.4(2), N(1)−Li(1)−O(61) 126.4(3), N(12)−Li(1)−N(22) 127.5(3), B(1)−N(1)−B(2) 113.2(2), N(1)−B(1)−N(31) 101.1(2), N(1)−B(2)−N(32) 100.5(2); N(1)B(1)B(2)//B(1)B(2)N(31)N(32) 8.1.

effect of the Li^+ or Mg^{2+} ion likely leads to $[\mathbf{L^1}]^-$ formation.

The ^{1}H NMR spectra of [Li(thf)$\mathbf{L^1}$] and [Mg(Cl)(thf)$_x$-$\mathbf{L^1}$] show similar characteristics as the spectrum of H$\mathbf{L^1}$: One signal for the NMe protons, two sets of signals for terminal and bridging pyrazolyl rings (integral ratio = 2:1, respectively), as well as signals for the phenyl moieties (integral ratio pz/Ph = 9:10). The ^{1}H NMR spectra of [Mg(Cl)(thf)$_x\mathbf{L^1}$] and [Mg(Cl)(thf)$_2\mathbf{L^2}$] are also pretty much alike, apart from the fact that the NMe resonance is missing in the latter case.

The ^{11}B NMR resonances of [Li(thf)$\mathbf{L^1}$], [Mg(Cl)(thf)$_x$-$\mathbf{L^1}$], and [Mg(Cl)(thf)$_2\mathbf{L^2}$] appear at 6.7 ppm, 5.3 ppm, and 5.4 ppm, respectively, thereby testifying to the presence of four-coordinate boron nuclei in all three compounds.[34]

The molecular structure of the lithium complex was determined by X-ray crystallography. The compound, which is monomeric in the solid state, crystallizes with two crystallographically independent molecules in the asymmetric unit ([Li(thf)$\mathbf{L^1}$] and [Li(thf)$\mathbf{L^1}$]$_A$). Since the key geometric parameters of both molecules are the same within the experimental error margins, only the structure of [Li(thf)$\mathbf{L^1}$] is discussed here (Figure 4; Table 1).

As in the [*N*,*O*,*N*] complex [Li(thf)$\mathbf{L^2}$],[30] the Li^+ center in [Li(thf)$\mathbf{L^1}$] possesses a coordination number of four: $[\mathbf{L^1}]^-$ acts as tridentate ligand, the fourth coordination site is occupied by a THF molecule. However, replacement of the B−O−B bridge by a B−N(Me)-B fragment causes an increase in the N(12)−Li(1)−N(22) angle by 11.6° ([Li(thf)$\mathbf{L^1}$]: N(12)−Li(1)−N(22) = 127.5(3)°).

Lithiation of H$\mathbf{L^1}$ significantly flattens the envelope conformation of the N(1)B(1)B(2)N(31)N(32) ring; the corresponding dihedral angles N(1)B(1)B(2)//B(1)B(2)N(31)N(32) are 31.5° in H$\mathbf{L^1}$, but only 8.1° in [Li(thf)$\mathbf{L^1}$]. Moreover, the average B−N(Me) bond length shrinks by 0.071 Å from a value of 1.600(4) Å in H$\mathbf{L^1}$ to 1.529(4) Å in [Li(thf)$\mathbf{L^1}$]. This shortening of the B−N(Me) bonds is accompanied by a significant increase in the mean B(1)−N(11)/B(2)−N(21) distances upon going from H$\mathbf{L^1}$ (1.542(4) Å) to [Li(thf)$\mathbf{L^1}$] (1.584(4) Å). In contrast, the B−N(μ-pz) bond lengths remain the same (1.586(4) Å in H$\mathbf{L^1}$; 1.588(4) Å in [Li(thf)$\mathbf{L^1}$]). This observation is in line with previous findings of negative hyperconjugation in amino-substituted pyrazaboles $R_2N(R')B(\mu\text{-pz})_2B(R')NR_2$[35,36] and lends support to our suggestion that deprotonation of H$\mathbf{L^1_B}$ promotes dissociation of terminal pyrazolyl groups and thus ultimately causes a rearrangement to [Li(thf)$\mathbf{L^1}$] (see above).

The magnesium complex [Mg(Cl)(thf)$_x\mathbf{L^1}$], which was crystallized from pentane/THF, forms chloride-bridged dinuclear aggregates [$\mathbf{L^1}$Mg(μ-Cl)$_2$Mg(thf)$\mathbf{L^1}$] in the solid state (Figure 5; Table 1).

The Mg(1) ion is five-coordinate by the donor atoms N(1), N(12), and N(22) of $[\mathbf{L^1}]^-$ and by the two bridging chloride ions. According to the structure parameter τ_5 = 0.44,[37] the configuration of the ligand environment is intermediate between trigonal-bipyramidal and square-pyramidal. In contrast to Mg(1), the Mg(2) ion bears an additional thf ligand and thus possesses a slightly distorted octahedral donor environment. Most importantly, $[\mathbf{L^1}]^-$ acts as meridionally coordinating tridentate chelator toward Mg(2), the angle N(62)−Mg(2)−N(72) = 158.5(1)° being even more obtuse than N(12)−Mg(1)−N(22) = 139.3(1)°.

With regard to the key structure parameters of the ligand backbone, we note that the average B−N(Me) bond length (1.546(2) Å) in [$\mathbf{L^1}$Mg(μ-Cl)$_2$Mg(thf)$\mathbf{L^1}$] lies between the average B−N(Me) distances in H$\mathbf{L^1}$ (1.600(4) Å) and [Li(thf)$\mathbf{L^1}$] (1.529(4) Å). The same is true for the mean terminal B−N(pz) bond lengths (H$\mathbf{L^1}$: 1.542(4) Å, [$\mathbf{L^1}$Mg(μ-Cl)$_2$Mg(thf)$\mathbf{L^1}$]: 1.572(2) Å, [Li(thf)$\mathbf{L^1}$]: 1.584(4) Å). This comparison leads to the conclusion that the negative hyperconjugation from the central amino group into the B−N(pz) σ* orbitals is less pronounced in the magnesium complex than in the lithium species, which is most likely due to the higher Lewis acidity of the Mg^{2+} ion compared to that of the Li^+ ion.

Crystals of [Mg(Cl)(thf)$_2\mathbf{L^2}$] have been grown from a pentane/THF mixture (cf. the Supporting Information for an ORTEP-plot and a compilation of key structure parameters of [Mg(Cl)(thf)$_2\mathbf{L^2}$]). In contrast to

(34) Nöth, H.; Wrackmeyer, B. Nuclear Magnetic Resonance Spectroscopy of Boron Compounds. In *NMR Basic Principles and Progress*; Diehl, P., Fluck, E., Kosfeld, R., Eds.; Springer: Berlin, 1978.

(35) Jäkle, F.; Priermeier, T.; Wagner, M. *Organometallics* **1996**, *15*, 2033–2040.

(36) Herdtweck, E.; Jäkle, F.; Opromolla, G.; Spiegler, M.; Wagner, M.; Zanello, P. *Organometallics* **1996**, *15*, 5524–5535.

(37) For five-coordinate complexes, the geometry index $\tau_5 = (\theta - \varphi)/60°$ provides a quantitative measure of whether the ligand sphere more closely approaches a square-pyramidal ($\tau_5 = 0$) or a trigonal-bipyramidal geometry ($\tau_5 = 1$; θ, φ are the two largest bond angles and $\theta \geq \varphi$): Addison, A. W.; Rao, T. N.; Reedijk, J.; van Rijn, J.; Verschoor, G. C. *J. Chem. Soc., Dalton Trans.* **1984**, 1349–1356.

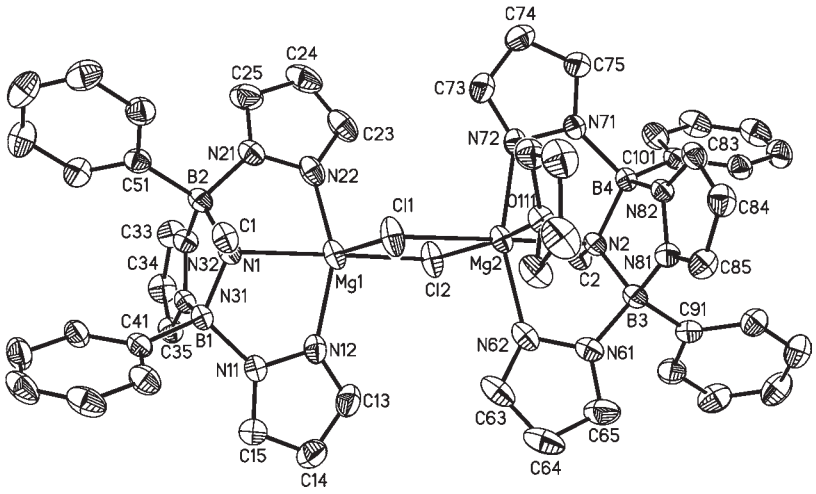

Figure 5. Molecular structure of $[\mathbf{L^1}Mg(\mu\text{-}Cl)_2Mg(thf)\mathbf{L^1}]$. The H-atoms are omitted for clarity; displacement ellipsoids are drawn at the 50% probability level. Selected bond lengths [Å] and angles [deg]: Mg(1)−Cl(1) 2.384(1), Mg(1)−Cl(2) 2.443(1), Mg(2)−Cl(1) 2.563(1), Mg(2)−Cl(2) 2.531(1), Mg(1)−N(1) 2.268(2), Mg(1)−N(12) 2.078(2), Mg(1)−N(22) 2.074(2), Mg(2)−N(2) 2.293(2), Mg(2)−N(62) 2.098(2), Mg(2)−N(72) 2.099(2), Mg(2)−O(111) 2.258(1), B(1)−N(1) 1.549(2), B(1)−N(11) 1.569(3), B(2)−N(1) 1.550(3), B(2)−N(21) 1.570(2), B(3)−N(2) 1.541(2), B(3)−N(61) 1.577(2), B(4)−N(2) 1.542(2), B(4)−N(71) 1.573(2); Cl(1)−Mg(1)−Cl(2) 89.4(1), Cl(1)−Mg(2)−Cl(2) 83.6(1), Mg(1)−Cl(1)−Mg(2) 93.8(1), Mg(1)−Cl(2)−Mg(2) 93.2(1), Cl(1)−Mg(1)−N(1) 105.1(1), Cl(2)−Mg(1)−N(1) 165.5(1), N(12)−Mg(1)−N(22) 139.3(1), Cl(1)−Mg(2)−N(2) 177.8(1), Cl(2)−Mg(2)−N(2) 97.9(1), N(62)−Mg(2)−N(72) 158.5(1).

$[\mathbf{L^1}Mg(\mu\text{-}Cl)_2Mg(thf)\mathbf{L^1}]$, $[Mg(Cl)(thf)_2\mathbf{L^2}]$ forms discrete mononuclear complexes in the crystal lattice. The distorted octahedral ligand sphere of the Mg^{2+} ion in $[Mg(Cl)(thf)_2\mathbf{L^2}]$ is composed of $[\mathbf{L^2}]^-$, one Cl^- ion, and two thf ligands. A striking difference between $[\mathbf{L^1}Mg(\mu\text{-}Cl)_2Mg(thf)\mathbf{L^1}]$ and $[Mg(Cl)(thf)_2\mathbf{L^2}]$ lies in the fact that $[\mathbf{L^2}]^-$ is clearly facially coordinating (N(pz)−Mg−N(pz)′ = 90.5(1)°).

Investigation into the Conformational Flexibility of $[\mathbf{L^1}]^-$ and $[\mathbf{L^2}]^-$: $[Zn(Br)\mathbf{L^1}]$, $[Zn(Br)(Hpz)\mathbf{L^2}]$, and $[Cu(Cl)\mathbf{L^1}]$. Since classic tridentate poly(pyrazol-1-yl)borates are restricted to facial binding modes, the meridional coordination of $[\mathbf{L^1}]^-$ in $[\mathbf{L^1}Mg(\mu\text{-}Cl)_2Mg(thf)\mathbf{L^1}]$ prompted us to begin a systematic investigation into the conformational flexibility of fourth generation scorpionates.

For our studies, we selected the following target complexes: $[Zn(Br)\mathbf{L^1}]$, $[Zn(Br)\mathbf{L^2}]$, and $[Cu(Cl)\mathbf{L^1}]$ ($[Cu(Cl)\mathbf{L^2}]$ has already been described by our group).[30] The rationale behind this selection was that four-coordinate Zn^{II} complexes are usually tetrahedral, which should force $[\mathbf{L^1}]^-/[\mathbf{L^2}]^-$ into a *fac*-like conformation, while four-coordinate Cu^{II} complexes tend to adopt square-planar coordination geometries and thus should promote a *mer*-like conformation of $[\mathbf{L^1}]^-/[\mathbf{L^2}]^-$.

Complex $[Zn(Br)\mathbf{L^1}]$ was prepared in a two-step sequence: First, $H\mathbf{L^1}$ was treated with 1 equiv of $ZnBr_2$ in THF. The mixture was stirred for 2 h to achieve precoordination of $ZnBr_2$ to $H\mathbf{L^1}$. In the second step, 1 equiv of *n*-BuLi in hexane was added at −78 °C which resulted in deprotonation of the central amino group, accompanied by elimination of LiBr and formation of the target compound (Scheme 2).

Attempts to prepare the related complex $[Zn(Br)\mathbf{L^2}]$ from the [*N*,*O*,*N*] ligand $[Li(thf)\mathbf{L^2}]$ and $ZnBr_2$ reproducibly resulted in the formation of the pyrazole adduct $[Zn(Br)(Hpz)\mathbf{L^2}]$ (Scheme 2). The compound was isolated by crystallization in yields of about 30%. Given that the pyrazole ligand obviously originates from degradation of $[\mathbf{L^2}]^-$, we tried to increase the yield of $[Zn(Br)(Hpz)\mathbf{L^2}]$ by adding 2 equiv of pyrazole to the mixture of starting materials. Indeed, this time $[Zn(Br)(Hpz)\mathbf{L^2}]$ formed almost quantitatively (^1H, ^{11}B NMR spectroscopic control). It should, however, be noted, that other N-donors like pyridine or 2,6-lutidine do not prevent ligand degradation. For example, reaction of $[Li(thf)\mathbf{L^2}]$ with $ZnBr_2$ in the presence of pyridine gave $[Zn(Br)(Hpz)\mathbf{L^2}]$ in the same yield as has been obtained without added base. Replacement of $ZnBr_2$ by $ZnCl_2$ also had no decisive effect on the course of the reaction because again only the pyrazole adduct $[Zn(Cl)(Hpz)\mathbf{L^2}]$ was generated (details of the synthesis of $[Zn(Cl)(Hpz)\mathbf{L^2}]$ and $[Zn(Br)(Hpz)\mathbf{L^2}]$ are given in the Supporting Information).

Scheme 2. Synthesis of $[Zn(Br)\mathbf{L^1}]$, $[Zn(Br)(Hpz)\mathbf{L^2}]$, and $[Cu(Cl)\mathbf{L^1}]$[a]

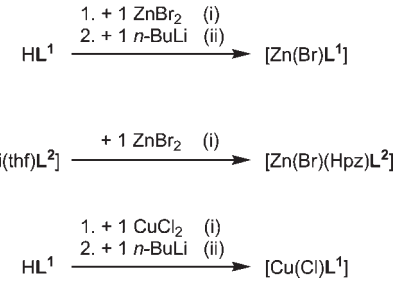

[a] (i) THF, r.t.; (ii) THF/hexane, −78 °C.

The deep blue Cu^{II} complex $[Cu(Cl)\mathbf{L^1}]$ was synthesized by adding 1 equiv of *n*-BuLi to a dark green mixture of $H\mathbf{L^1}$ and $CuCl_2$ in THF at −78 °C (Scheme 2).

The NMR data of $[Zn(Br)\mathbf{L^1}]$ nicely compare to those of $[Li(thf)\mathbf{L^1}]$ and $[Mg(Cl)(thf)_x\mathbf{L^1}]$ and will thus not be discussed further. Similarly, the NMR spectra of $[Zn(Br)(Hpz)\mathbf{L^2}]$ agree with those of $[Mg(Cl)(thf)_2\mathbf{L^2}]$, apart from the resonances of the pyrazole ligand, which appear at 6.33 ppm (HpzH-4), 7.28/8.09 ppm (HpzH-3,5), and 12.29 ppm (NH).

The molecular structures of $[Zn(Br)\mathbf{L^1}]$ and $[Cu(Cl)\mathbf{L^1}]$ are juxtaposed in Figure 6; key crystallographic data are compiled in Table 2 (cf. the Supporting Information for

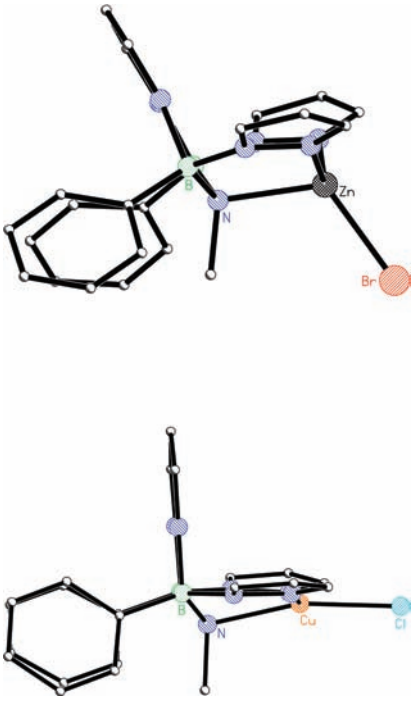

Figure 6. Comparison of the molecular structures of [Zn(Br)$\mathbf{L^1}$] and [Cu(Cl)$\mathbf{L^1}$] in the solid state.

Table 2. Selected Crystallographic Data of [Zn(Br)$\mathbf{L^1}$] and [Cu(Cl)$\mathbf{L^1}$]

compound	[Zn(Br)$\mathbf{L^1}$]·2C_4H_8O	[Cu(Cl)$\mathbf{L^1}$]
formula	$C_{30}H_{38}B_2BrN_7O_2Zn$	$C_{22}H_{22}B_2ClCuN_7$
fw	695.57	505.08
color, shape	colorless, block	dark blue, block
temperature (K)	173(2)	173(2)
crystal system	triclinic	triclinic
space group	$P\bar{1}$	$P\bar{1}$
a (Å)	11.951(2)	10.8061(11)
b (Å)	12.826(3)	12.8424(14)
c (Å)	13.559(3)	18.620(2)
α (deg)	69.40(3)	73.420(8)
β (deg)	63.85(3)	74.722(8)
γ (deg)	62.23(3)	87.420(8)
V (Å^3)	1622.4(6)	2387.8(4)
Z	2	4
$D_{calcd.}$ (g cm^{-3})	1.424	1.405
$F(000)$	716	1036
μ (mm^{-1})	2.027	1.051
crystal size (mm^3)	0.31 × 0.28 × 0.22	0.25 × 0.22 × 0.22
no. of rflns collected	22313	18290
no. of indep rflns (R_{int})	5722 (0.0913)	8877 (0.0927)
data/restraints/parameters	5722/0/389	8877/0/595
GOF on F^2	1.081	1.042
$R1$, $wR2$ ($I > 2\sigma(I)$)	0.0689, 0.1763	0.0649, 0.1668
$R1$, $wR2$ (all data)	0.0806, 0.1941	0.0859, 0.1799
largest diff peak and hole (e Å^{-3})	1.265, −1.554	0.732, −1.124

ORTEP plots and a compilation of important bond lengths and angles of [Zn(Br)$\mathbf{L^1}$] and [Cu(Cl)$\mathbf{L^1}$]; the X-ray crystal structure analysis of [Zn(Cl)(Hpz)$\mathbf{L^2}$] and [Zn(Br)(Hpz)$\mathbf{L^2}$] are also given in the Supporting Information).

The Zn(1) center in [Zn(Br)$\mathbf{L^1}$] is surrounded by the [$\mathbf{L^1}$]$^-$ ligand and one Br$^-$ ion. The sum of the bond angles Br−Zn−N(pz), Br−Zn−N(pz)′, and N(pz)−Zn−N(pz)′ is 355.8°. If the ligand configuration about Zn was an ideal tetrahedron, the corresponding value would have to be 328.5°; in the case of an ideal trigonal pyramid with N(Me) occupying the axial position, we would expect an angle sum of 360.0° in the basal plane. In line with that, the geometry index τ_4[38] of [Zn(Br)$\mathbf{L^1}$] has a value of 0.82, typical of a (distorted) trigonal-pyramidal configuration.

Scheme 3. Synthesis of [$CoCl_2$(H$\mathbf{L^1}$)] and [$\mathbf{L^1}$Co(μ-Cl)$_2$Co$\mathbf{L^1}$][a]

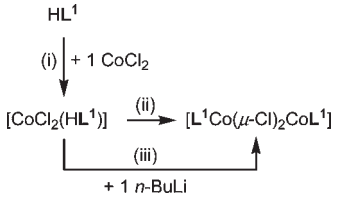

[a] (i) THF, r.t., subsequent recrystallization from CH_2Cl_2/hexane at r.t.; (ii) CH_2Cl_2/hexane, 7 d; (iii) THF/hexane, −78 °C.

X-ray crystallography on [Cu(Cl)$\mathbf{L^1}$] reveals a monomeric compound with a four-coordinate Cu^{II} center, in contrast to the solid-state structure of the related [*N*,*O*,*N*] complex [Cu(Cl)$\mathbf{L^2}$],[30] which consists of chloro-bridged dimeric entities [Cu(Cl)$\mathbf{L^2}$]$_2$ containing five-coordinate Cu^{II} ions. The geometry of the ligand environment in [Cu(Cl)$\mathbf{L^1}$] is largely square-planar, with N(pz)−Cu−N(pz)′ and Cl−Cu−N(Me) angles of 161.5(2)° and 165.8(1)°, respectively. When these values are compared to the corresponding angles of [Zn(Br)$\mathbf{L^1}$] (N(pz)−Zn−N(pz)′ = 127.2(3)°, Br−Zn(1)−N(Me) = 117.7(2)°), an astonishingly high degree of conformational flexibility of ligand [$\mathbf{L^1}$]$^-$ becomes immediately apparent.

Importantly, the different coordination modes are *not* accompanied by any major changes in the bond lengths and angles of the central NB_2N_2 five-membered ring. With regard to octahedral complexes, we may therefore safely assume, that [$\mathbf{L^1}$]$^-$ is able to bind both in a facial and in a meridional manner.

Ligand Properties of HL^1 versus [L^1]$^-$: [CoCl$_2$(HL^1)] and [L^{1}Co(μ-Cl)$_2$CoL^1]. In the course of the synthesis of [Zn(Br)$\mathbf{L^1}$] and [Cu(Cl)$\mathbf{L^1}$] it has become apparent that treatment of a mixture of the respective metal salt and H$\mathbf{L^1}$ with *n*-BuLi leads to better results than the reaction between the same metal salt and [Li(thf)$\mathbf{L^1}$]. However, we have not yet been able to isolate the likely intermediates of the sequential protocol, that is, [$ZnBr_2$(H$\mathbf{L^1}$)] and [$CuCl_2$(H$\mathbf{L^1}$)].

This situation changed when $CoCl_2$ was employed. The products of both synthesis steps, the protonated species [$CoCl_2$(H$\mathbf{L^1}$)] and the deprotonated complex [$\mathbf{L^1}$Co(μ-Cl)$_2$Co$\mathbf{L^1}$], are described in this paragraph.

[$CoCl_2$(H$\mathbf{L^1}$)] readily forms from $CoCl_2$ and H$\mathbf{L^1}$ in THF (Scheme 3). Deep blue crystals of [$CoCl_2$(H$\mathbf{L^1}$)] were grown from CH_2Cl_2/hexane. After these crystals had been stored in the mother liquor for a period of several days, we discovered that the color of the entire crop had changed from blue to violet. Subsequent X-ray crystallography revealed the complete conversion of [$CoCl_2$(H$\mathbf{L^1}$)] into [$\mathbf{L^1}$Co(μ-Cl)$_2$Co$\mathbf{L^1}$]. As to be expected, this process can be accelerated by adding 1 equiv of *n*-BuLi to

(38) For four-coordinate complexes, the geometry index $\tau_4 = \{360° - (\theta+\varphi)\}/141°$ provides a quantitative measure of whether the ligand sphere more closely approaches a tetrahedral ($\tau_4 = 1$) or a trigonal-pyramidal geometry ($\tau_4 = 0.85$; θ, φ are the two largest bond angles): Yang, L.; Powell, D. R.; Houser, R. P. *Dalton Trans.* **2007**, 955–964.

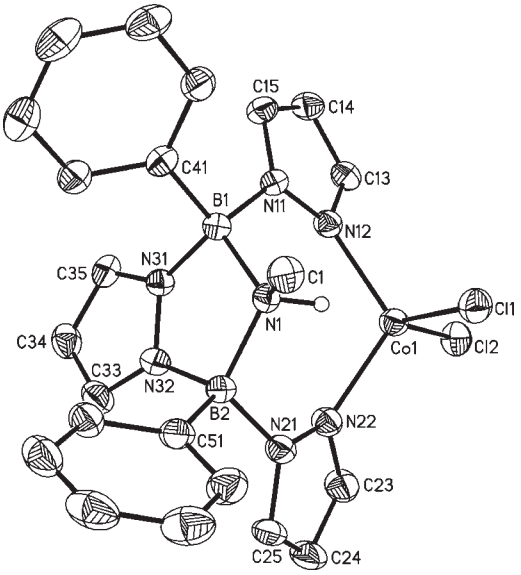

Figure 7. Molecular structure of $[CoCl_2(H\mathbf{L}^1)]$. The H-atoms are omitted for clarity (except H(1) on the N(Me) bridge); displacement ellipsoids are drawn at the 50% probability level. Selected bond lengths [Å], atom···atom distances [Å], angles [deg], and dihedral angles [deg]: Co(1)−Cl(1) 2.264(1), Co(1)−Cl(2) 2.257(1), Co(1)−N(12) 2.024(2), Co(1)−N(22) 2.035(2), Co(1)···N(1) 3.179(2), Cl(1)···H(1) 2.45(4), B(1)−N(1) 1.617(4), B(1)−N(11) 1.553(4), B(2)−N(1) 1.623(4), B(2)−N(21) 1.559(4); Cl(1)−Co(1)−Cl(2) 116.0(1), N(12)−Co(1)−N(22) 112.8(1), B(1)−N(1)−B(2) 110.5(2); N(1)B(1)B(2)//B(1)B(2)N(31)N(32) 8.9.

Table 3. Selected Crystallographic Data of $[CoCl_2(H\mathbf{L}^1)]$ and $[\mathbf{L}^1Co(\mu\text{-}Cl)_2Co\mathbf{L}^1]$

compound	$[CoCl_2(H\mathbf{L}^1)]$	$[\mathbf{L}^1Co(\mu\text{-}Cl)_2Co\mathbf{L}^1]\cdot CH_2Cl_2$
formula	$C_{22}H_{23}B_2Cl_2CoN_7$	$C_{45}H_{46}B_4Cl_4Co_2N_{14}$
fw	536.92	1085.86
color, shape	blue, plate	violet, plate
temperature (K)	173(2)	173(2)
crystal system	triclinic	monoclinic
space group	$P\bar{1}$	$P2_1/c$
a (Å)	9.2228(9)	10.1326(6)
b (Å)	9.9006(9)	22.9453(11)
c (Å)	14.4611(13)	11.8089(8)
α (deg)	96.443(7)	90
β (deg)	105.370(7)	110.323(5)
γ (deg)	96.724(8)	90
V (Å^3)	1250.2(2)	2574.6(3)
Z	2	2
$D_{calcd.}$ (g cm^{-3})	1.426	1.401
$F(000)$	550	1112
μ (mm^{-1})	0.925	0.899
crystal size (mm^3)	0.22 × 0.18 × 0.09	0.27 × 0.19 × 0.11
no. of rflns collected	18031	37037
no. of indep rflns (R_{int})	4688 (0.0719)	5168 (0.0833)
data/restraints/parameters	4688/0/311	5168/0/316
GOF on F^2	0.932	1.025
$R1$, $wR2$ ($I > 2\sigma(I)$)	0.0385, 0.0810	0.0481, 0.1258
$R1$, $wR2$ (all data)	0.0609, 0.0881	0.0655, 0.1329
largest diff peak and hole (e Å^{-3})	0.470, −0.549	0.715, −1.243

the THF solution of $[CoCl_2(H\mathbf{L}^1)]$ prior to workup (Scheme 3).

Complex $[CoCl_2(H\mathbf{L}^1)]$ is a monomeric compound featuring one Co^{II} center in a distorted tetrahedral environment (Figure 7; Table 3; the hydrogen atom H(1) has been located in the electron density map).

The average B−N(Me) bond length of 1.620(4) Å is similar to that of $H\mathbf{L}^1$ (1.600(4) Å), but almost 0.1 Å longer than that of $[Li(thf)\mathbf{L}^1]$ (1.529(4) Å). On the other hand, the N(1)B(1)B(2)N(31)N(32) ring in $[CoCl_2(H\mathbf{L}^1)]$ was found to be rather flat (N(1)B(1)B(2)//B(1)B(2)N(31)N(32) = 8.9°), which is similar to $[Li(thf)\mathbf{L}^1]$ (8.1°), but different from $H\mathbf{L}^1$ (31.5°).

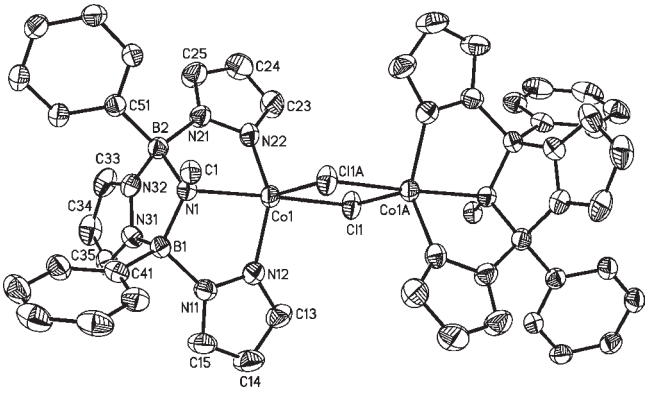

Figure 8. Molecular structure of $[\mathbf{L}^1Co(\mu\text{-}Cl)_2Co\mathbf{L}^1]$. The H-atoms are omitted for clarity; displacement ellipsoids are drawn at the 50% probability level. Selected bond lengths [Å] and angles [deg]: Co(1)−Cl(1) 2.515(1), Co(1)−Cl(1A) 2.329(1), Co(1)−N(1) 2.228(2), Co(1)−N(12) 1.995(2), Co(1)−N(22) 1.993(2), B(1)−N(1) 1.550(4), B(1)−N(11) 1.572(4), B(2)−N(1) 1.552(4), B(2)−N(21) 1.576(4); Cl(1)−Co(1)−Cl(1A) 87.1(1), N(12)−Co(1)−N(22) 132.1(1), B(1)−N(1)−B(2) 110.6(2). Symmetry transformation used to generate equivalent atoms: A: $-x+1$, $-y+1$, $-z$.

Deprotonation of $[CoCl_2(H\mathbf{L}^1)]$ is accompanied by the formation of a third Co−N bond (Co(1)−N(1) = 2.228(2) Å) and loss of one chloro ligand (Figure 8; Table 3). In the solid state, the new complex exists as centrosymmetric dimer $[\mathbf{L}^1Co(\mu\text{-}Cl)_2Co\mathbf{L}^1]$ with five-coordinate Co^{II} ions in a distorted trigonal-bipyramidal environment ($\tau_5 = 0.63$[37]). The average Co−N(pz) bond length is smaller in $[\mathbf{L}^1Co(\mu\text{-}Cl)_2Co\mathbf{L}^1]$ (1.994(2) Å) as compared to $[CoCl_2(H\mathbf{L}^1)]$ (2.030(2) Å), but the N(12)−Co(1)−N(22) angle is more obtuse by almost 20°.

The X-ray crystal structure analysis of $[CoCl_2(H\mathbf{L}^1)]$ reveals why HCl abstraction does not necessarily require an external base, but happens spontaneously: The proton on N(1) is directed toward the midpoint of the Co(1)−Cl(1) bond and the distance Cl(1)···H(1) amounts to only 2.45(4) Å. An intramolecular proton shift from N(1) to Cl(1) can therefore easily take place.

In view of the successful synthesis of $[\mathbf{L}^1Co(\mu\text{-}Cl)_2Co\mathbf{L}^1]$, we also tried to prepare the corresponding complex $[\mathbf{L}^2Co(\mu\text{-}Cl)_2Co\mathbf{L}^2]$ from $CoCl_2$ and $[Li(thf)\mathbf{L}^2]$. However, this reaction always proceeded with degradation of some of the $[N,O,N]$ ligands and yielded compound $[\mathbf{L}^2Co(\mu\text{-}Cl)(\mu\text{-}pz)Co\mathbf{L}^2]$ which possesses a bridging pyrazolide ring (cf. the Supporting Information for the synthesis and X-ray crystal structure analysis of $[\mathbf{L}^2Co(\mu\text{-}Cl)(\mu\text{-}pz)Co\mathbf{L}^2]$).

Investigation into the Chemical Stability of $[\mathbf{L}^1]^-$ and $[\mathbf{L}^2]^-$: $[Mn(CO)_3\mathbf{L}^2]$, $K(thf)[Mn(CO)_3\mathbf{L}^3]$, and $[\mathbf{L}^2Co(\mu\text{-}pz)_2Co\mathbf{L}^2]$. The above-mentioned formation of the pyrazole and μ-pyrazolide complexes $[Zn(Cl,Br)(Hpz)\mathbf{L}^2]$ and $[\mathbf{L}^2Co(\mu\text{-}Cl)(\mu\text{-}pz)Co\mathbf{L}^2]$ poses questions regarding the general chemical stability of $[\mathbf{L}^1]^-$ and $[\mathbf{L}^2]^-$. In the past, we had observed similar ligand degradation reactions when trying to prepare $[(R_2Bpz_2)Mn(CO)_4]$ complexes from classic bis(pyrazol-1-yl)borates and $[Mn(CO)_5Br]$.[18] Thus, to gather more information about the stability limits of fourth generation scorpionates, we

Scheme 4. Synthesis of $[Mn(CO)_3\mathbf{L^2}]$ and $K(thf)[Mn(CO)_3\mathbf{L^3}]$[a]

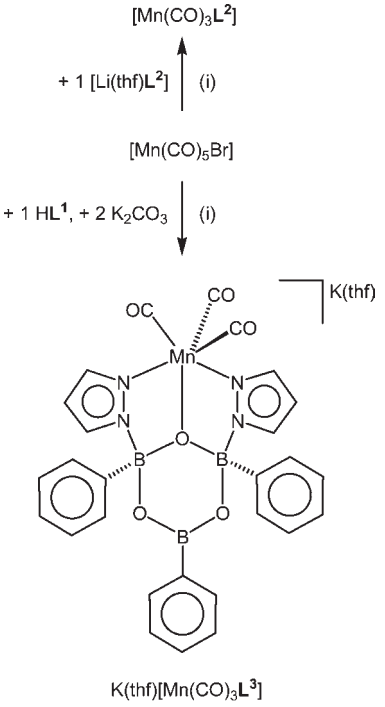

[a] (i) THF, reflux temperature, 8 h.

decided to treat also $[\mathbf{L^1}]^-$ and $[\mathbf{L^2}]^-$ with the manganese carbonyl reagent.

Attempts at the synthesis of $[Mn(CO)_3\mathbf{L^1}]$ from an equimolar mixture of $[Li(thf)\mathbf{L^1}]$ and $[Mn(CO)_5Br]$ in THF at reflux temperature met with failure because the ligand framework does not persist under these conditions. In an alternative approach and similar to the preparation of $[Zn(Br)\mathbf{L^1}]$ and $[\mathbf{L^1}Co(\mu\text{-}Cl)_2Co\mathbf{L^1}]$, we used $H\mathbf{L^1}$ and performed the experiment in the presence of a base (*n*-BuLi, NEt_3, K_2CO_3). None of these reactions gave evidence for the formation of $[Mn(CO)_3\mathbf{L^1}]$. However, in the case where K_2CO_3 (2 equiv) was employed, we isolated an interesting other product in moderate yield (i.e., $K(thf)[Mn(CO)_3\mathbf{L^3}]$; Scheme 4). This compound contains a new ligand, $[\mathbf{L^3}]^{2-}$, featuring a three-atom O−B(Ph)−O backbone instead of a two-atom μ-pyrazolide bridge. $K(thf)[Mn(CO)_3\mathbf{L^3}]$ is relatively air-stable in the solid state, but its THF and CH_2Cl_2 solutions are air-sensitive.

In a previous publication, we have already reported on a related system, that is, $[(p\text{-cymene})Ru\mathbf{L^3}]$, which has been synthesized from $[(p\text{-cymene})RuCl_2]_2$ and $[Li(thf)\mathbf{L^2}]$ in the presence of $TlPF_6$ (1:2:4 equiv, respectively).[39] In the case of $[(p\text{-cymene})Ru\mathbf{L^3}]$, two pathways can be envisaged for the formation of the boroxine ligand $[\mathbf{L^3}]^{2-}$: (i) a rearrangement reaction of $[\mathbf{L^2}]^-$ and (ii) hydrolysis of $[\mathbf{L^2}]^-$ by adventitious traces of water. In the case of $K(thf)[Mn(CO)_3\mathbf{L^3}]$, however, water (probably originating from the hygroscopic K_2CO_3) must be the key factor, because it is the only plausible source of oxygen atoms in the entire setup.

The serendipitous discovery of $K(thf)[Mn(CO)_3\mathbf{L^3}]$ led us to attempt a targeted synthesis of the anionic complex from $Li[Li(thf)\mathbf{L^3}]$[39] and $[Mn(CO)_5Br]$ in THF. However, this synthesis protocol, which has been shown to work faithfully for the preparation of $[(p\text{-cymene})Ru\mathbf{L^3}]$,[39] failed for the manganese compound because we only isolated $[Mn_2(CO)_{10}]$, the product of a $Mn^I \rightarrow Mn^0$ reduction, from the reaction mixture.

In contrast to $H\mathbf{L^1}$, $[Li(thf)\mathbf{L^2}]$ reacts with 1 equiv of $[Mn(CO)_5Br]$ (THF, reflux, 8 h) without degradation so that the target compound $[Mn(CO)_3\mathbf{L^2}]$ is obtained in 70% yield (Scheme 4). Recrystallization of $[Mn(CO)_3\mathbf{L^2}]$ from Et_2O led to yellow crystals suitable for X-ray analysis. The compound is relatively air-stable, even in solution (Et_2O, CH_2Cl_2), but rapidly decomposes on a silica gel chromatography column.

The ^{11}B NMR spectrum of $K(thf)[Mn(CO)_3\mathbf{L^3}]$ is characterized by two signals at about 31 ppm ($h_{1/2} \approx 1100$ Hz, 1B) and 6.1 ppm (2B), which confirm that the molecule contains three- and four-coordinate boron atoms.[34] The ^1H NMR spectrum is consistent with the presence of two magnetically equivalent pyrazolyl rings ($\delta(^1H)$ = 6.24 (pzH-4), 7.65, 7.81 (pzH-3,5)) as well as three phenyl groups, two of them being again magnetically equivalent.

Compound $[Mn(CO)_3\mathbf{L^2}]$ gives rise to one resonance at $\delta(^{11}B) = 6.0$. Two sets of ^1H (^{13}C) signals can be assigned to one symmetrically bridging pyrazolyl ring on the one hand and two metal-coordinating pyrazolyl substituents on the other.

The IR spectrum of $[Mn(CO)_3\mathbf{L^2}]$ exhibits one sharp and one broad band in the typical region of CO stretching vibrations. The corresponding wavenumbers ($\tilde{\nu}$ (CO) = 2033 cm^{-1}, 1930 cm^{-1}; KBr) compare well with those of $Mn(CO)_3$ complexes of classic tris(pyrazol-1-yl)borate ligands.[18,40,41] In contrast to $[Mn(CO)_3\mathbf{L^2}]$, *three* sharp absorptions at $\tilde{\nu}$ (CO) = 2026 cm^{-1}, 1929 cm^{-1}, and 1891 cm^{-1} are resolved in the IR spectrum (KBr) of $K(thf)[Mn(CO)_3\mathbf{L^3}]$.

The cyclic voltammograms of complexes $[Mn(CO)_3\mathbf{L^2}]$ and $K(thf)[Mn(CO)_3\mathbf{L^3}]$ show irreversible $Mn^I \rightarrow Mn^{II}$ oxidation waves at E_{pa} = 0.69 and 0.86 V, respectively (vs FcH/FcH^+, CH_2Cl_2, NBu_4PF_6; see the Supporting Information for the CV plots). Thus, the negatively charged species $[Mn(CO)_3\mathbf{L^3}]^-$ is more resistant to oxidation than neutral $[Mn(CO)_3\mathbf{L^2}]$. The electrochemical behavior of $[Mn(CO)_3\mathbf{L^2}]$ and $K(thf)[Mn(CO)_3\mathbf{L^3}]$ may be compared with that of the related cyclopentadienyl complex $[CpMn(CO)_3]$, which undergoes reversible one-electron oxidation at a potential value of $E_{1/2}$ = 0.89 V (vs FcH/FcH^+, CH_2Cl_2, NBu_4PF_6).[42,43]

The molecular structures of $[Mn(CO)_3\mathbf{L^2}]$ and $K(thf)[Mn(CO)_3\mathbf{L^3}]$ are presented in Figures 9 and 10, respectively (see also Table 4).

In both complexes, the Mn^I ion is located in a distorted octahedral environment composed of three facially coordinating carbonyl ligands and the [*N*,*O*,*N*] donor set of the respective chelate ligand. The Mn−CO bonds of

(39) Mutseneck, E. V.; Reus, C.; Schödel, F.; Bolte, M.; Lerner, H.-W.; Wagner, M. *Organometallics* **2010**, *29*, 966−975.

(40) Joachim, J. E.; Apostolidis, C.; Kanellakopulos, B.; Maier, R.; Marques, N.; Meyer, D.; Müller, J.; de Matos, A. P.; Nuber, B.; Rebizant, J.; Ziegler, M. L. *J. Organomet. Chem.* **1993**, *448*, 119–129.

(41) Haghiri Ilkhechi, A.; Guo, S.; Bolte, M.; Wagner, M. *Dalton Trans.* **2003**, 2303–2307.

(42) Atwood, C. G.; Geiger, W. E.; Bitterwolf, T. E. *J. Electroanal. Chem.* **1995**, *397*, 279–285.

(43) Laws, D. R.; Chong, D.; Nash, K.; Rheingold, A. L.; Geiger, W. E. *J. Am. Chem. Soc.* **2008**, *130*, 9859–9870.

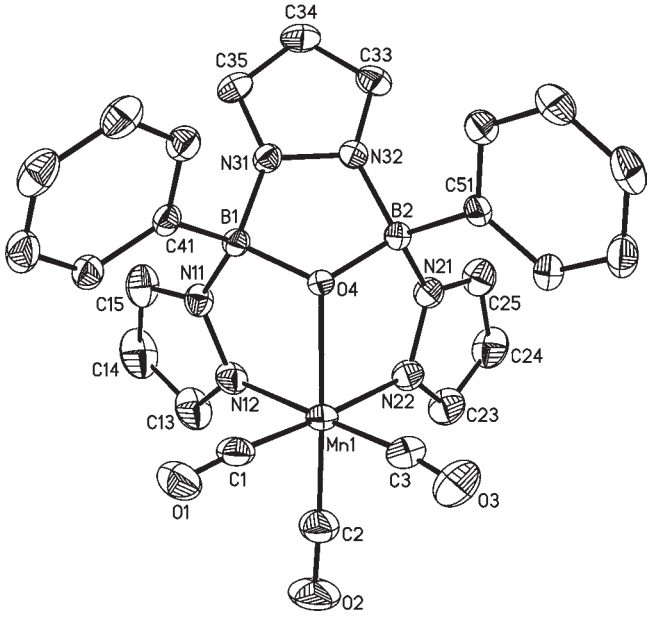

Figure 9. Molecular structure of $[Mn(CO)_3\mathbf{L^2}]$. The H-atoms are omitted for clarity; displacement ellipsoids are drawn at the 50% probability level. Selected bond lengths [Å] and angles [deg]: Mn(1)−O(4) 2.091(1), Mn(1)−N(12) 2.038(1), Mn(1)−N(22) 2.055(1), Mn(1)−C(1) 1.820(2), Mn(1)−C(2) 1.803(2), Mn(1)−C(3) 1.825(2), B(1)−O(4) 1.486(2), B(2)−O(4) 1.490(2), B(1)−N(11) 1.563(2), B(1)−N(31) 1.566(2), B(2)−N-(21) 1.560(2), B(2)−N(32) 1.573(2); N(12)−Mn(1)−N(22) 87.3(1).

$[Mn(CO)_3\mathbf{L^2}]$ involving carbonyl ligands *trans* to the pyrazolyl rings are slightly longer (1.820(2) Å, 1.825(2) Å) than the Mn(1)−C(2) bond *trans* to O(4) (1.803(2) Å). This leads to the conclusion that the oxygen atom acts not only as σ-, but also as π-donor. A similar effect is visible in the boroxine derivative K(thf)$[Mn(CO)_3\mathbf{L^3}]$ (Mn(1)−C(4) = 1.829(2) Å vs Mn(1)−C(5) = 1.793(2) Å; C(6)O-(6) is not taken into account here, because it bridges Mn(1) and K(1A)). The Mn−O and average Mn−N bond lengths of K(thf)$[Mn(CO)_3\mathbf{L^3}]$ (Mn−O = 2.079(1) Å, Mn−N = 2.032(2) Å) are a little shorter than those of $[Mn(CO)_3\mathbf{L^2}]$ (Mn−O = 2.091(1) Å, Mn−N = 2.047(1) Å), most likely because of a higher electrostatic attraction of the dianionic ligand $[\mathbf{L^3}]^{2-}$ compared to the mono-anionic (pyrazol-1-yl)borate $[\mathbf{L^2}]^-$.

K(thf)$[Mn(CO)_3\mathbf{L^3}]$ forms heterobimetallic coordination polymers in the solid state (cf. the Supporting Information for a plot of the extended structure). The connecting K^+ ions bind to the boroxine oxygen atom O(2) and the phenyl carbon atoms C(41)/C(42) of one $[Mn(CO)_3\mathbf{L^3}]^-$ complex and at the same time to the phenyl ring (η^6-mode) and the carbonyl oxygen atom O(6A) of a second $[Mn(CO)_3\mathbf{L^3}]^-$ anion.[44] The coordination sphere of each K^+ ion is completed by one thf ligand.

The structure parameters of the chelate ligands in $[Mn(CO)_3\mathbf{L^2}]$ and $[Mn(CO)_3\mathbf{L^3}]^-$ nicely fit to those in $[Mg(Cl)(thf)_2\mathbf{L^2}]$ and [(*p*-cymene)Ru$\mathbf{L^3}$][39] and thus do not merit further discussion.

(44) For more examples of $L_nM-CO\cdots K^+$ bonding interactions, see: (a) Wink, D. J.; Fox, J. R.; Cooper, N. J. *J. Am. Chem. Soc.* **1985**, *107*, 5012–5014. (b) Himmel, D.; Seitz, M.; Scheer, M. *Z. Anorg. Allg. Chem.* **2004**, *630*, 1220–1228. (c) Kirin, V.; Roesky, P. W. *Eur. J. Inorg. Chem.* **2004**, 1045–1050. (d) Aldridge, S.; Baker, R. J.; Coombs, N. D.; Jones, C.; Rose, R. P.; Rossin, A.; Willock, D. J. *Dalton Trans.* **2006**, 3313–3320. (e) Kunz, K.; Vitze, H.; Bolte, M.; Lerner, H.-W.; Wagner, M. *Organometallics* **2007**, *26*, 4663–4672.

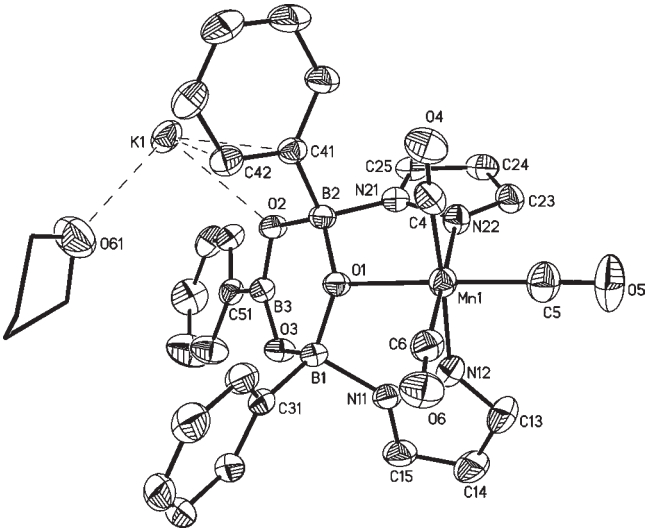

Figure 10. Molecular structure of K(thf)$[Mn(CO)_3\mathbf{L^3}]$. The H-atoms are omitted for clarity; displacement ellipsoids are drawn at the 50% probability level. Selected bond lengths [Å] and angles [deg]: Mn(1)−O(1) 2.079(1), Mn(1)−N(12) 2.029(2), Mn(1)−N(22) 2.035(2), Mn(1)−C(4) 1.829(2), Mn(1)−C(5) 1.793(2), Mn(1)−C(6) 1.794(2), K(1)−O(2) 2.693(1), K(1)-O(6A) 2.898(2), K(1)−C(41) 3.198(2), K(1)−C(42) 3.119(2), K-(1)···COG(Ph(31A)) 2.986, B(1)−O(1) 1.473(2), B(1)−O(3) 1.459(3), B-(2)−O(1) 1.484(2), B(2)−O(2) 1.469(3), B(3)−O(2) 1.365(3), B(3)−O(3) 1.348(3), B(1)−N(11) 1.595(3), B(2)−N(21) 1.575(3); N(12)−Mn(1)−N-(22) 88.7(1), B(1)−O(1)−B(2) 121.1(2). COG(Ph(31A)) = centroid of the phenyl ring containing C(31A). Symmetry transformation used to generate equivalent atoms: A: $x - 1/2, -y + 1/2, z - 1/2$.

Table 4. Selected Crystallographic Data of $[Mn(CO)_3\mathbf{L^2}]$ and K(thf)$[Mn(CO)_3\mathbf{L^3}]$

compound	$[Mn(CO)_3\mathbf{L^2}]$	K(thf)$[Mn(CO)_3\mathbf{L^3}]$
formula	$C_{24}H_{19}B_2MnN_6O_4$	$C_{31}H_{29}B_3KMnN_4O_7$
fw	532.01	696.05
color, shape	yellow, block	yellow, block
temperature (K)	173(2)	173(2)
crystal system	monoclinic	monoclinic
space group	$P2_1/c$	$P2_1/n$
a (Å)	10.8977(6)	11.4093(3)
b (Å)	19.1699(7)	17.8054(6)
c (Å)	12.8863(6)	17.0313(5)
α (deg)	90	90
β (deg)	111.739(4)	105.180(2)
γ (deg)	90	90
V (Å^3)	2500.6(2)	3339.14(17)
Z	4	4
$D_{calcd.}$ (g cm^{-3})	1.413	1.385
$F(000)$	1088	1432
μ (mm^{-1})	0.571	0.571
crystal size (mm^3)	0.41 × 0.36 × 0.33	0.28 × 0.26 × 0.25
no. of rflns collected	38051	43379
no. of indep rflns (R_{int})	5750 (0.0462)	6804 (0.0535)
data/restraints/parameters	5750/0/335	6804/26/421
GOF on F^2	1.032	1.061
$R1$, $wR2$ ($I > 2\sigma(I)$)	0.0308, 0.0807	0.0424, 0.1043
$R1$, $wR2$ (all data)	0.0354, 0.0832	0.0498, 0.1084
largest diff peak and hole (e Å^{-3})	0.324, −0.399	0.551, −0.452

The unexpected formation of K(thf)$[Mn(CO)_3\mathbf{L^3}]$ prompted us to unveil important factors governing the assembly of $[\mathbf{L^3}]^{2-}$. In the absence of K^+ and $[Mn(CO)_5Br]$, hydrolysis of $H\mathbf{L^1}$ gives the bridged pyrazabole PhB(μ-pz)$_2$(μ-OB(Ph)O)BPh.[29] In the presence of both, K^+ ions *and* $[Mn(CO)_5Br]$, a pyrazolide-boroxine diadduct ($[\mathbf{L^3}]^{2-}$) is formed. To see the effect of K^+ ions alone, we kept a mixture of $H\mathbf{L^1}$ and K_2CO_3 (stoichiometric ratio = 1:5) in

Scheme 5. Synthesis of $[K(thf)_2L^4]$[a]

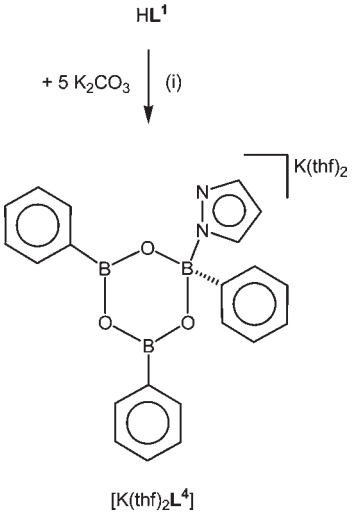

[a] (i) THF, reflux temperature, 8 h.

THF for 8 h at reflux temperature. After workup, colorless crystals were obtained.

The ^{1}H NMR spectrum of the sample in THF-d_8 is characterized by few broad signals indicating dynamic behavior of the species in solution.

According to X-ray crystallography, the crystals consist of the potassium salt of a phenylboroxine-pyrazolide monoadduct (i.e., $[K(thf)_2\mathbf{L^4}]$; Scheme 5), which crystallizes in the form of dimers $[K(thf)_2\mathbf{L^4}]_2$ (cf. the Supporting Information for more details of the synthesis and the molecular structure of $[K(thf)_2\mathbf{L^4}]_2$).

These results lead to the conclusion that K^+ ions are able to shift the course of $H\mathbf{L^1}$ hydrolysis from pyrazabole to boroxine formation. However, $[K(thf)_2\mathbf{L^4}]$ contains only one pyrazolide donor per boroxine ring, which is consistent with the view that 1:1 adducts, but not 1:2 adducts, between boroxine and amines are thermodynamically favorable.[45−49] In the case of $K(thf)[Mn(CO)_3\mathbf{L^3}]$, a driving force for the generation of the boroxine-pyrazolide diadduct is most likely provided by $Mn(CO)_3$ chelation (*note*: the lithium salt $Li[Li(thf)\mathbf{L^3}]$ also features a boroxine-pyrazolide diadduct, and, similar to $K(thf)[Mn(CO)_3\mathbf{L^3}]$, the Li^+ ion is chelated by the two pyrazolyl rings and one boroxine oxygen atom).[39]

We find it noteworthy in this context, that *partial* hydrolysis of only the B−N(Me)-B fragment, but *not* the B-(μ-pz)-B backbone, has been observed upon treatment of $H\mathbf{L^1}$ with K_2CO_3 (1.5 equiv) in the presence of $CoCl_2$ (1 equiv). The resulting complex $[\mathbf{L^2}Co(\mu\text{-pz})_2Co\mathbf{L^2}]$ (Scheme 6) was isolated in almost 25% yield (cf. the Supporting Information for more details of the synthesis procedure and an X-ray crystal structure analysis).

Scheme 6. Reaction Between $H\mathbf{L^1}$, K_2CO_3, and $CoCl_2$ with Formation of $[\mathbf{L^2}Co(\mu\text{-pz})_2Co\mathbf{L^2}]$[a]

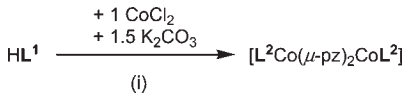

[a] (i) THF, r.t., 12 h.

Given that replacement of N(Me) by O in the central part of the ligand framework requires a considerable degree of bond breaking and reforming, it can be concluded that $[\mathbf{L^1}]^-$ and $[\mathbf{L^2}]^-$ possess substantial self-healing forces, as long as the amount of water is limited, and pyrazolide ions are not trapped by transition metal Lewis acids.

Rearrangement of the [*N*,*O*,*N*] pyrazolylborate $[\mathbf{L^{2Ph}}]^-$. As already stated in the introductory paragraph, a major advantage of classic tris(pyrazol-1-yl)borate donors lies in the fact that it is conveniently possible to tune their steric demand by introducing bulky substituents into the 3-positions of the pyrazolyl rings (i.e., $[HB(^{3R}pz)_3]^-$). With the aid of these so-called, "second generation scorpionates", even highly reactive metal complex fragments can be kinetically stabilized.[1] Sometimes, however, such regiochemically pure scorpionate ligands have been observed to undergo ring-flip isomerization to $[HB(^{5R}pz)_n(^{3R}pz)_{3-n}]^-$ during complex formation.[1]

Also in the case of our ligand systems, the selective synthesis of 3-substituted derivatives has been achieved (e.g., $[Li(thf)\mathbf{L^{2Ph}}]$; Scheme 7).[30] This immediately raises questions into the configurational stability of these ligands when strong transition metal Lewis acids are present.

Given this background, it is revealing to compare the outcome of the reaction between $FeCl_3$ and $[Li(thf)\mathbf{L^2}]$ on the one hand and $[Li(thf)\mathbf{L^{2Ph}}]$ on the other.

In the first case, the expected compound $[FeCl_2\mathbf{L^2}]$ was obtained in 71% yield after recrystallization.[30] In the second case, however, we isolated complex $[FeCl_2(^{3Ph}pzH)\mathbf{L^5}]$ (Scheme 7). The compound was characterized by X-ray crystallography (cf. the Supporting Information for details of the synthesis and the X-ray crystal structure analysis of $[FeCl_2(^{3Ph}pzH)\mathbf{L^5}]$).

$[FeCl_2(^{3Ph}pzH)\mathbf{L^5}]$ contains an Fe^{III} ion in a slightly distorted octahedral coordination environment. The (pyrazol-1-yl)borate $[\mathbf{L^5}]^-$ acts as facially coordinating tridentate ligand. The remaining three coordination sites are occupied by two chloride ions and one 3-phenylpyrazole molecule (Scheme 7). $[FeCl_2(^{3Ph}pzH)\mathbf{L^5}]$ is remarkable in several respects: (i) $B-N(^{3Ph}pz)$ bonds have been broken so that free 3-phenylpyrazole is available for iron coordination. (ii) A 3-phenylpyrazolyl ring has moved from a terminal to the sterically more encumbered bridging position. (iii) The ratio ^{3Ph}pz:pz of 2:1 in $[Li(thf)\mathbf{L^2}]$ has changed to 1:2 in $[\mathbf{L^5}]^-$. $[\mathbf{L^5}]^-$ is therefore not just the product of intraligand pyrazole shuffling, but it must have been assembled from the fragments of at least two $[\mathbf{L^2}]^-$ molecules.

These observations indicate $[\mathbf{L^{2Ph}}]^-$ to be a rather dynamic molecule in solution because it readily undergoes B−N dissociation and reassociation. The same might even be true for the parent ligand $[\mathbf{L^2}]^-$, for which such equilibria are harder to detect, because the compound possesses only one sort of pyrazolyl rings. The

(45) Beckmann, J.; Dakternieks, D.; Duthie, A.; Lim, A. E. K.; Tiekink, E. R. T. *J. Organomet. Chem.* **2001**, *633*, 149–156.
(46) Perttu, E. K.; Arnold, M.; Iovine, P. M. *Tetrahedron Lett.* **2005**, *46*, 8753–8756.
(47) Iovine, P. M.; Gyselbrecht, C. R.; Perttu, E. K.; Klick, C.; Neuwelt, A.; Loera, J.; DiPasquale, A. G.; Rheingold, A. L.; Kua, J. *Dalton Trans.* **2008**, 3791–3794.
(48) Kua, J.; Iovine, P. M. *J. Phys. Chem. A* **2005**, *109*, 8938–8943.
(49) Kua, J.; Fletcher, M. N.; Iovine, P. M. *J. Phys. Chem. A* **2006**, *110*, 8158–8166.

Scheme 7. Ligand Rearrangement upon Treatment of [Li(thf)$\mathbf{L^{2Ph}}$] with $FeCl_3$[a]

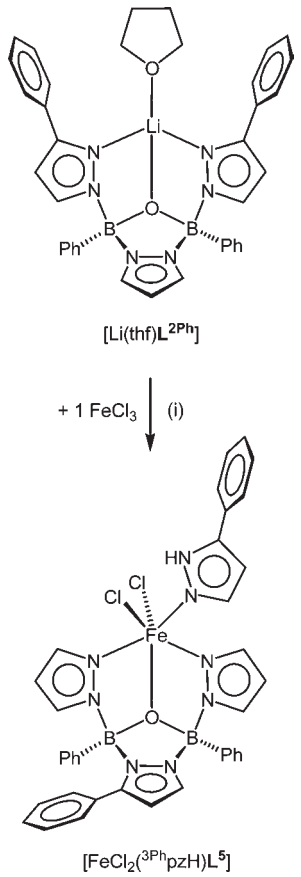

[a] (i) THF, r.t., 10 h.

structural fluxionality of $\mathbf{L^2}$-type compounds can be rationalized by considering the π-donor ability of the central oxygen atom which helps to stabilize three-coordinate boron intermediates generated by B−N dissociation.

Conclusion

This paper deals with the coordination properties of fourth generation scorpionates, that is, mixed-donor (pyrazol-1-yl)-borates with potentially large bite angles. We started our investigation with the [*N*,*N*,*N*]/[*N*,*O*,*N*] ligands [Ph(pz)B(μ-N(Me))(μ-pz)B(pz)Ph]$^-$ ($[\mathbf{L^1}]^-$)/[Ph(pz)B(μ-O)(μ-pz)B(pz)-Ph]$^-$($[\mathbf{L^2}]^-$) and included main group metal ions (Li^+, Mg^{2+}) as well as middle (Mn^I, Co^{II}) and late transition metal ions (Cu^{II}, Zn^{II}) into the study.

Li^+ and Mg^{2+} complexes are accessible with both ligands (i.e., [Li(thf)$\mathbf{L^1}$], [Li(thf)$\mathbf{L^2}$], [Mg(Cl)(thf)$_x\mathbf{L^1}$], [Mg(Cl)(thf)$_2$-$\mathbf{L^2}$], and the same is true for Cu^{II} ([Cu(Cl)$\mathbf{L^1}$], [Cu(Cl)$\mathbf{L^2}$]). In contrast, Zn^{II} ions undergo clean complexation only with $[\mathbf{L^1}]^-$ ([Zn(Br)$\mathbf{L^1}$]), while the reactions between ZnX_2 (X = Cl, Br) and [Li(thf)$\mathbf{L^2}$] proceeded with decomposition of a part of the ligand molecules and yielded the pyrazole complexes [Zn(X)(Hpz)$\mathbf{L^2}$].

We noted on several occasions that treatment of $[\mathbf{L^1}]^-$ with certain metal reagents led to ligand degradation (e.g., with $MgCl_2$) or unwanted redox reactions (e.g., with [$Mn(CO)_5$-Br]). In some of these cases, the problem could be solved by applying a sequential protocol: First, the acid H$\mathbf{L^1}$ was mixed with the metallic component and in a second step *n*-BuLi was added as a base.

Using $CoCl_2$, it was possible to isolate and fully characterize both the intermediate [$CoCl_2$(H$\mathbf{L^1}$)] and the final product [$\mathbf{L^1}$Co(μ-Cl)$_2$Co$\mathbf{L^1}$] of the reaction sequence. Interestingly, HCl elimination from [$CoCl_2$(H$\mathbf{L^1}$)] does not necessarily require the assistance of a base, but happens spontaneously when a solution of the complex is stored at room temperature for several days. Similar to the case of Zn^{II}, attempts to prepare Co^{II} complexes of $[\mathbf{L^2}]^-$ were accompanied by ligand decomposition and gave the pyrazolyl-bridged dinuclear compound [$\mathbf{L^2}$Co(μ-Cl)(μ-pz)Co$\mathbf{L^2}$].

Efforts to synthesize the Mn^{II} complex [$Mn(CO)_3\mathbf{L^1}$] from [$Mn(CO)_5$Br] and either [Li(thf)$\mathbf{L^1}$] or H$\mathbf{L^1}$ in the presence of a base (*n*-BuLi, NEt_3, K_2CO_3) all met with failure. With K_2CO_3, however, we isolated the compound K(thf)[Mn-$(CO)_3\mathbf{L^3}$] from the reaction mixture. K(thf)[$Mn(CO)_3\mathbf{L^3}$] features another example of a fourth generation scorpionate, that is, the boroxine-based [*N*,*O*,*N*] derivative [Ph(pz)B(μ-O)(μ-OB(Ph)O)B(pz)Ph]$^{2-}$($[\mathbf{L^3}]^{2-}$). $[\mathbf{L^3}]^{2-}$ is undoubtedly a hydrolysis product of $[\mathbf{L^1}]^-$; we believe that the source of water was the hygroscopic K_2CO_3. The fact, that the boroxine adduct $[\mathbf{L^3}]^{2-}$ is assembled under reaction conditions that otherwise lead to the degradation of H$\mathbf{L^1}$ underlines the high stability of $[\mathbf{L^3}]^{2-}$ and suggests to employ this ligand deliberately in future studies ($Li_2[\mathbf{L^3}]$ is easily accessible from 2 Lipz and $(B(Ph)O)_3$).[39] In contrast to [$Mn(CO)_3\mathbf{L^1}$], the [*N*,*O*,*N*] congener [$Mn(CO)_3\mathbf{L^2}$] forms from [$Mn(CO)_5$Br] and [Li(thf)$\mathbf{L^2}$] in excellent yields.

As evidenced by the crystal structure analyses of the complexes [Zn(Br)$\mathbf{L^1}$]/[Mg(Cl)(thf)$_2\mathbf{L^2}$]/[$Mn(CO)_3\mathbf{L^2}$] on the one hand and [$\mathbf{L^1}$Mg(μ-Cl)$_2$Mg(thf)$\mathbf{L^1}$]/[Cu(Cl)$\mathbf{L^1}$]/[Cu-(Cl)$\mathbf{L^2}$]$_2$ on the other, $[\mathbf{L^1}]^-$ and $[\mathbf{L^2}]^-$ are able to adopt both a *fac* and a *mer* conformation, which is a unique feature in scorpionate chemistry.

Finally, we discovered that the ligand framework of $[\mathbf{L^1}]^-$ and $[\mathbf{L^2}]^-$ has a tendency to undergo B−N association/dissociation equilibrium reactions, most likely because the bridging *N*(Me) or O atom is able to stabilize three-coordinate boron intermediates by N/O−B π interactions. However, once chelation of a transition metal ion has been achieved, the resulting complexes are reasonably stable, in many cases even toward air and moisture.

Experimental Section

General Considerations. All reactions were carried out under nitrogen using standard Schlenk techniques. All solvents were dried and distilled prior to use. Ligand [Li(thf)$\mathbf{L^2}$] was prepared as published in the literature.[30] ^{1}H, ^{11}B{^{1}H}, and ^{13}C{^{1}H} NMR spectra were recorded on Bruker AMX 300 or Avance 400 spectrometers at room temperature. Abbreviations: s = singlet, d = doublet, t = triplet, vt = virtual triplet, dd = doublet of doublets, m = multiplet, n.r. = multiplet not resolved, br = broad, Me = methyl, Ph = phenyl, pz = pyrazol-1-yl. IR: Jasko FT-IR 4200 spectrometer. Cyclic voltammograms were recorded using an EG&G Princeton Applied Research 263A potentiostat. Elemental analyses were performed by the microanalytical laboratory of the Goethe University Frankfurt.

Synthesis of H$\mathbf{L^1}$. A mixture of ($Me_2N(Ph)B)_2$NMe (1.61 g, 5.49 mmol) and Hpz (0.90 g, 13.22 mmol) was refluxed in Et_2O (20 mL) for 12 h. The colorless precipitate formed was isolated by filtration, washed with Et_2O (3 × 10 mL), dried under vacuum and recrystallized from hexane/benzene. Yield: 1.36 g (76%; *note*: the sample still contained about 20% of H$\mathbf{L^1_B}$).

Crystals of H**L**^{1} suitable for X-ray analysis were obtained from a hexane/benzene mixture. ^{1}H NMR (300.0 MHz, $CDCl_3$): δ 2.28 (d, 3H, $^{3}J_{HH}$ = 5.7 Hz; NMe), 6.30 (vt, 2H; pzH-4), 6.57 (t, 1H, $^{3}J_{HH}$ = 2.4 Hz; μ-pzH-4), 7.04−7.07, 7.12−7.20 (2 × m, 4H, 6H; PhH), 7.44 (m, 4H; μ-pzH-3,5, pzH-3 or 5), 7.82 (d, 2H, $^{3}J_{HH}$ = 1.2 Hz; pzH-3 or 5), 8.40 (br, 1H; NH). ^{11}B{^{1}H} NMR (96.3 MHz, $CDCl_3$): δ 3.2.

Synthesis of [Li(thf)L^{1}]. A stirred solution of H**L**^{1} (420 mg, 1.03 mmol) in THF (5 mL) was treated at −78 °C with a 1.6 M solution of *n*-BuLi in hexane (0.63 mL, 1.01 mmol). The mixture was allowed to warm to room temperature and stirred overnight. Gas-phase diffusion of pentane into the solution led to colorless X-ray quality crystals within one week. The mother liquor was decanted and the crystals dried under vacuum. Yield: 470 mg (96%). ^{1}H NMR (300.0 MHz, THF-d_8): δ 1.99 (s, 3H; NMe), 6.22 (dd, 2H, $^{3}J_{HH}$ = 1.8, 2.3 Hz; pzH-4), 6.42 (t, 1H, $^{3}J_{HH}$ = 2.2 Hz; μ-pzH-4), 6.96−7.08 (m, 10H; PhH), 7.43 (d, 2H, $^{3}J_{HH}$ = 2.2 Hz; μ-pzH-3,5), 7.48 (dd, 2H, $^{4,3}J_{HH}$ = 0.6, 2.3 Hz; pzH-3 or 5), 7.55 (dd, 2H, $^{4,3}J_{HH}$ = 0.6, 1.8 Hz; pzH-3 or 5). ^{11}B{^{1}H} NMR (96.3 MHz, THF-d_8): δ 6.7. ^{13}C{^{1}H} NMR (75.5 MHz, THF-d_8): δ 33.2 (NMe), 105.4 (pzC-4), 109.2 (μ-pzC-4), 126.4 (PhC-*p*), 127.1 (PhC-*m*), 131.0 (μ-pzC-3,5), 134.0 (PhC-*o*), 134.7, 139.1 (pzC-3,5). Anal. Calcd for $C_{26}H_{30}B_2LiN_7O$ [485.13]: C, 64.37; H, 6.23; N, 20.21. Found: C, 64.57; H, 6.23; N, 20.40.

Synthesis of [Mg(Cl)(thf)$_x$L^{1}]. A stirred solution of H**L**^{1} (177 mg, 0.43 mmol) in THF (5 mL) was treated at −78 °C with a 3 M solution of MeMgCl in THF (0.14 mL, 0.42 mmol). The reaction mixture was allowed to warm to room temperature and stirred overnight. It was then concentrated to a volume of 2 mL under vacuum and layered with pentane, whereupon colorless crystals formed that were suitable for X-ray analysis ([**L**^{1}Mg(μ-Cl)$_2$Mg(thf)**L**^{1}]). The mother liquor was decanted, and the crystals dried under vacuum. Yield: 220 mg (97%). ^{1}H NMR (300.0 MHz, $CDCl_3$): δ 2.22 (s, 3H; NMe), 6.35 (vt, 2H; pzH-4), 6.51 (t, 1H, $^{3}J_{HH}$ = 2.4 Hz; μ-pzH-4), 6.96−7.05, 7.09−7.15 (2 × m, 4H, 6H; PhH), 7.33 (d, 2H, $^{3}J_{HH}$ = 2.4 Hz; μ-pzH-3,5), 7.48, 7.86 (d, n.r., 2 × 2H, $^{3}J_{HH}$ = 2.1 Hz; pzH-3,5). ^{11}B{^{1}H} NMR (96.3 MHz, $CDCl_3$): δ 5.3.

Synthesis of [Mg(Cl)(thf)$_2$L^{2}]. A mixture of [Li(thf)**L**^{2}] (113 mg, 0.24 mmol) and anhydrous $MgCl_2$ (22 mg, 0.23 mmol) was stirred in THF (10 mL) overnight. Gas-phase diffusion of pentane into the solution led to colorless X-ray quality crystals within 2 weeks. The mother liquor was removed using a syringe, and the crystals were dried under vacuum. Yield: 121 mg (88%). ^{1}H NMR (300.0 MHz, $CDCl_3$): δ 6.38 (vt, 2H; pzH-4), 6.60 (t, 1H, $^{3}J_{HH}$ = 2.4 Hz; μ-pzH-4), 6.88−6.94, 7.02−7.14 (2 × m, 4H, 6H; PhH), 7.58 (dd, 2H, $^{4,3}J_{HH}$ = 0.6, 2.1 Hz; pzH-3 or 5), 7.68 (d, 2H, $^{3}J_{HH}$ = 2.4 Hz; μ-pzH-3,5), 8.01 (d, 2H, $^{3}J_{HH}$ = 1.8 Hz; pzH-3 or 5). ^{11}B{^{1}H} NMR (96.3 MHz, THF-d_8): δ 5.4. Anal. Calcd for $C_{29}H_{35}B_2ClMgN_6O_3$ [597.01]: C, 58.34; H, 5.91; N, 14.07. Found: C, 58.07; H, 5.96; N, 14.19.

Synthesis of [Zn(Br)L^{1}]. A mixture of H**L**^{1} (230 mg, 0.56 mmol) and $ZnBr_2$ (126 mg, 0.56 mmol) in THF (10 mL) was stirred at room temperature for 2 h. The mixture was cooled to −78 °C, a 1.6 M solution of *n*-BuLi in hexane (0.35 mL, 0.56 mmol) was added, the temperature was allowed to rise to room temperature, and stirring was continued overnight (*note*: *n*-BuLi can be replaced by $NaN(SiMe_3)_2$). The reaction mixture was concentrated under reduced pressure to a volume of 2 mL and layered with pentane, whereupon colorless crystals formed that were suitable for X-ray analysis. The mother liquor was decanted, and the crystals were dried under vacuum. Yield: 190 mg (59%). ^{1}H NMR (300.0 MHz, $CDCl_3$): δ 2.00 (s, 3H; NMe), 6.48 (vt, 2H; pzH-4), 6.54 (t, 1H, $^{3}J_{HH}$ = 2.1 Hz; μ-pzH-4), 7.02−7.09, 7.20−7.25 (2 × m, 4H, 6H; PhH), 7.37 (d, 2H, $^{3}J_{HH}$ = 2.1 Hz; μ-pzH-3,5), 7.62, 7.84 (2×dd, 2×2H, $^{4,3}J_{HH}$ = 0.6, 2.0/2.4 Hz; pzH-3,5). ^{1}B{^{1}H} NMR (96.3 MHz, $CDCl_3$): δ 5.1. ^{13}C{^{1}H} NMR (75.4 MHz, $CDCl_3$): δ 39.1 (NMe), 108.2 (pzC-4), 110.6 (μ-pzC-4), 127.4 (PhC-*m*), 127.6 (PhC-*p*), 131.0 (μ-pzC-3,5), 133.4 (PhC-*o*), 135.0, 139.3 (pzC-3,5). Anal. Calcd for $C_{22}H_{22}B_2BrN_7Zn$ [551.35] × 0.33 C_4H_8O [72.11]: C, 48.70; H, 4.32; N, 17.04. Found: C, 48.81; H, 4.45; N, 17.03 (*note*: the relative amount of THF was confirmed by ^{1}H NMR spectroscopy).

Synthesis of [Cu(Cl)L^{1}]. H**L**^{1} (284 mg, 0.70 mmol) and $CuCl_2$ (94 mg, 0.70 mmol) were stirred in THF (5 mL) at room temperature for 2 h. The dark green solution formed was cooled to −78 °C. A 1.6 M solution of *n*-BuLi in hexane (0.45 mL, 0.72 mmol) was added, whereupon the color of the mixture changed to deep blue. The mixture was allowed to warm to room temperature, stirred for 2 h and then layered with hexane (20 mL). Dark blue X-ray quality crystals formed, which were collected on a frit, rinsed with hexane, and dried under vacuum. Yield: 95 mg (27%). Anal. Calcd for $C_{22}H_{22}B_2ClCuN_7$ [505.08]: C, 52.32; H, 4.39; N, 19.41. Found: C, 52.06; H, 4.50; N, 19.18%.

Synthesis of [CoCl$_2$(HL^{1})]. A mixture of H**L**^{1} (204 mg, 0.50 mmol) and $CoCl_2$ (65 mg, 0.50 mmol) was stirred in THF (10 mL) overnight. The resulting deep blue solution was evaporated to dryness, and the residue was extracted into CH_2Cl_2. The extract was concentrated to a volume of 3 mL and layered with hexane (20 mL). Blue crystals (suitable for X-ray analysis) formed, which were isolated by filtration, rinsed with hexane and dried under vacuum. *Note*: The blue crystals should be isolated soon after they appear. Prolonged storage of the crystals in the mother liquor results in their transformation into crystals of [**L**^{1}Co(μ-Cl)$_2$Co**L**^{1}]. Yield: 215 mg (80%). Anal. Calcd for $C_{22}H_{23}B_2Cl_2CoN_7$ [536.92] × 0.75 CH_2Cl_2 [84.93]: C, 45.49; H, 4.11; N, 16.32. Found: C, 45.32; H, 4.38; N, 16.76. The identity of the entire sample with the material used for single crystal X-ray analysis was further confirmed by X-ray powder diffraction.

Synthesis of [L^{1}Co(μ-Cl)$_2$CoL^{1}]. A mixture of H**L**^{1} (204 mg, 0.50 mmol) and $CoCl_2$ (65 mg, 0.50 mmol) was stirred in THF (10 mL) for 2 h. The resulting dark blue solution was cooled to −78 °C, and a 1.6 M solution of *n*-BuLi in hexane (0.33 mL, 0.53 mmol) was added. The reaction mixture was allowed to warm to ambient temperature and stirred overnight. A black precipitate formed, which was removed by filtration. The violet filtrate was concentrated to a volume of 2 mL and layered with hexane (20 mL). Violet crystals (suitable for X-ray analysis) formed, which were collected on a frit, rinsed with hexane, and dried under vacuum. Yield: 105 mg (39%). Anal. Calcd for $C_{44}H_{44}B_4Cl_2Co_2N_{14}$ [1000.93] × CH_2Cl_2 [84.93]: C, 49.78; H, 4.27; N, 18.05. Found: C, 50.41; H, 4.28; N, 18.43.

Synthesis of K(thf)[Mn(CO)$_3$L^{3}]. A mixture of H**L**^{1} (194 mg, 0.48 mmol), [$Mn(CO)_5Br$] (131 mg, 0.48 mmol), and K_2CO_3 (133 mg, 0.96 mmol) in THF (10 mL) was heated at reflux temperature for 8 h. The resulting yellow suspension was cooled to room temperature and filtered through a frit. The filtrate was concentrated under reduced pressure to a volume of 3 mL and layered with hexane (20 mL). Yellow X-ray quality crystals formed, which were isolated by filtration and dried under vacuum. Yield: 104 mg (31% based on [$Mn(CO)_5Br$]). ^{1}H NMR (400.1 MHz, THF-d_8): δ 6.24 (vt, 2H; pzH-4), 7.18 (m, 2H; PhH-*p*), 7.25−7.36 (m, 7H; PhH-*m*, PhH*-*m*,*p*), 7.65 (n.r., 2H; pzH-3 or 5), 7.73 (m, 4H; PhH-*o*), 7.81 (d, 2H, $^{3}J_{HH}$ = 1.6 Hz; pzH-3 or 5), 7.96−8.01 (m, 2H; PhH*-*o*). ^{1}B{^{1}H} NMR (128.4 MHz, THF-d_8): δ 6.1 (s, 2B), 31 ($h_{1/2} \approx$ 1100 Hz, 1B). ^{13}C{^{1}H} NMR (62.9 MHz, THF-d_8): δ 105.7 (pzC-4), 126.0 (PhC-*p*), 127.3 (PhC-*m*), 127.6 (PhC*-*m*), 129.3 (PhC*-*p*), 132.2 (pzC-3 or 5), 133.0 (PhC-*o*), 135.0 (PhC*-*o*), 138.8 (pzC-3 or 5). IR (KBr, cm^{-1}): $\tilde{\nu}$ (CO) 2026, 1929, 1891. ESI-MS: *m*/*z* (%) 585.7 [M-(K(thf))]$^-$ (14), 529.6 [M-(K(thf))-2CO]$^-$ (12), 501.5 [M-(K(thf))-3CO]$^-$ (100). Anal. Calcd for $C_{31}H_{29}B_3KMnN_4O_7$ [696.05]: C, 53.49; H, 4.20; N, 8.05. Found: C, 53.31; H, 4.20; N, 8.03.

Synthesis of [Mn(CO)$_3$L^{2}]. A mixture of [Li(thf)**L**^{2}] (113 mg, 0.24 mmol) and [$Mn(CO)_5Br$] (63 mg, 0.23 mmol) in THF

(10 mL) was heated at reflux temperature for 8 h. The resulting solution was cooled to room temperature, all volatiles were removed under reduced pressure, and the crude product was extracted into CH_2Cl_2 (10 mL). The extract was evaporated to dryness under vacuum and the solid residue was recrystallized from Et_2O at −5 °C; the yellow crystals obtained were suitable for X-ray analysis. Yield: 88 mg (70%). ^{1}H NMR (400.1 MHz, $CDCl_3$): δ 6.35 (vt, 2H; pzH-4), 6.54 (t, 1H, $^3J_{HH}$ = 2.1 Hz; μ-pzH-4), 7.21−7.25, 7.29−7.34 (2 × m, 4H, 6H, PhH), 7.56, 7.63 (2 × d, 2 × 2H, 2 × $^3J_{HH}$ = 2.1 Hz; pzH-3 or 5, μ-pzH-3,5), 7.75 (d, 2H, $^3J_{HH}$ = 1.6 Hz; pzH-3 or 5). ^{1}B{^{1}H} NMR (128.4 MHz, $CDCl_3$): δ 6.0. ^{13}C{^{1}H} NMR (62.9 MHz, $CDCl_3$): δ 107.8 (pzC-4), 110.6 (μ-pzC-4), 127.6 (PhC-*m*), 128.1 (PhC-*p*), 131.0 (μ-pzC-3,5), 131.7 (pzC-3 or 5), 132.4 (PhC-*o*), 140.5 (pzC-3 or 5). IR (KBr, cm^{-1}): $\tilde{\nu}$(CO) 2033, 1930. ESI-MS: *m*/*z* (%) 533.3 $[M+H]^+$ (100). Anal. Calcd for $C_{24}H_{19}B_2MnN_6O_4$ [532.01]: C, 54.18; H, 3.60; N, 15.80. Found: C, 54.23; H, 3.73; N, 16.25.

X-ray Crystal Structure Analyses. Single crystals were analyzed with a STOE IPDS II two-circle diffractometer with graphite-monochromated MoK_α (0.71073 Å) radiation. Empirical absorption corrections were performed for all structures (except H**L**^{1} and [Li(thf)**L**^{1}]) using the MULABS[50] option in PLATON.[51] The structures were solved by direct methods using the program SHELXS[52] and refined against F^2 with full-matrix least-squares techniques using the program SHELXL-97.[53] All non-hydrogen atoms (except the disordered atoms of [Zn(Br)(Hpz)**L**^{2}]·C_4H_8O·0.5 C_6H_{14}, K(thf)[Mn(CO)$_3$**L**^{3}], and [K(thf)$_2$**L**^{4}]$_2$) were refined with anisotropic displacement parameters. The hydrogen atoms were geometrically positioned and treated as riding on the carbon atoms; the amino H atoms were freely refined.

In the absence of anomalous scatterers in [Li(thf)**L**^{1}], the Flack-*x*-parameter is meaningless. Therefore, Friedel pairs were merged and the absolute structure was arbitrarily set.

In [**L**^{1}Mg(μ-Cl)$_2$Mg(thf)**L**^{1}]·C_5H_{12}, the bond lengths in the pentane molecule were restrained to 1.5(1) Å, and the displacement parameters of the C atoms were restrained to an isotropic behavior.

The crystal lattice of [**L**^{2}Co(μ-Cl)(μ-pz)Co**L**^{2}]·CH_2Cl_2 contains void spaces. However, no significant electron density could be found in these regions.

In [**L**^{1}Co(μ-Cl)$_2$Co**L**^{1}]·CH_2Cl_2 the C atom of the CH_2Cl_2 molecule is disordered over two equally occupied positions.

The crystal of [Zn(Br)**L**^{1}]·2C_4H_8O was twinned (twin law: 1 0 0/1 −1 0/1 0 −1) with a ratio of 0.669(1)/0.331(1) for the two twin components.

In [Zn(Br)(Hpz)**L**^{2}]·C_4H_8O·0.5 C_6H_{14}, one atom of a non-coordinating THF molecule is disordered over two positions with a site occupation factor of 0.65(2) for the major occupied site.

For [Zn(Cl)(Hpz)**L**^{2}]·2C_4H_8O, the absolute structure was determined by refinement of the Flack-parameter: x = 0.03(3). One non-coordinating THF molecule in [Zn(Cl)-(Hpz)**L**^{2}]·2C_4H_8O is disordered over two positions with a site occupation factor of 0.70(2) for the major occupied site.

In K(thf)[Mn(CO)$_3$**L**^{3}] the coordinating thf molecule is disordered over two positions with a site occupation factor of 0.608(8) for the major occupied site.

In [K(thf)$_2$**L**^{4}]$_2$, two of the coordinating thf molecules show one disordered C atom each. These atoms are disordered over two positions with site occupation factors of 0.56(1) and 0.61(1) for the respective major occupied site.

Acknowledgment. Financial funding by the *Deutsche Forschungsgemeinschaft* (DFG) and the *Fonds der Chemischen Industrie* (FCI) is acknowledged. The authors are grateful to F. Schödel for cyclic voltammetric measurements.

Supporting Information Available: X-ray crystallographic files in CIF format. ORTEP-plot, selected structure parameters and crystallographic data of [Mg(Cl)(thf)$_2$**L**^{2}]. ORTEP plots and key structure parameters of [Zn(Br)**L**^{1}] and [Cu(Cl)**L**^{1}]. Synthesis and X-ray crystal structure analysis of [Zn(Cl)(Hpz)**L**^{2}], [Zn(Br)-(Hpz)**L**^{2}], and [**L**^{2}Co(μ-Cl)(μ-pz)Co**L**^{2}]. Plot of the polymeric structure of K(thf)[Mn(CO)$_3$**L**^{3}] in the solid state. Cyclic voltammograms of complexes [Mn(CO)$_3$**L**^{2}] and K(thf)[Mn(CO)$_3$**L**^{3}]. Synthesis and X-ray crystal structure analysis of [K(thf)$_2$**L**^{4}]$_2$, [**L**^{2}Co(μ-pz)$_2$Co**L**^{2}], and [FeCl$_2$(^{3Ph}pzH)**L**^{5}]. This material is available free of charge via the Internet at http://pubs.acs.org. Crystallographic data of H**L**^{1} (CCDC-758004), [Li(thf)**L**^{1}] (CCDC-758003), [**L**^{1}Mg(μ-Cl)$_2$Mg(thf)**L**^{1}] (CCDC-758005), [Mg(Cl)-(thf)$_2$**L**^{2}] (CCDC-758000), [Zn(Br)**L**^{1}] (CCDC-758007), [Zn(Br)-(Hpz)**L**^{2}] (CCDC-758002), [Zn(Cl)(Hpz)**L**^{2}] (CCDC-757997), [Cu(Cl)**L**^{1}] (CCDC-758006), [CoCl$_2$(H**L**^{1})] (CCDC-758008), [**L**^{1}Co(μ-Cl)$_2$Co**L**^{1}] (CCDC-758009), [**L**^{2}Co(μ-Cl)(μ-pz)Co**L**^{2}] (CCDC-758001), [**L**^{2}Co(μ-pz)$_2$Co**L**^{2}] (CCDC-758012), [Mn-(CO)$_3$**L**^{2}] (CCDC-757999), K(thf)[Mn(CO)$_3$**L**^{3}] (CCDC-758010), [K(thf)$_2$**L**^{4}]$_2$ (CCDC-758011), and [FeCl$_2$(^{3Ph}pzH)**L**^{5}] (CCDC-757998) in CIF format. These data can be obtained free of charge from the Cambridge Crystallographic Data Centre via www.ccdc.cam.ac.uk/data_request/cif.

(50) Blessing, R. H. *Acta Crystallogr.* **1995**, *A51*, 33–38.
(51) Spek, A. L. *J. Appl. Crystallogr.* **2003**, *36*, 7–13.
(52) Sheldrick, G. M. *Acta Crystallogr.* **1990**, *A46*, 467–473.
(53) Sheldrick, G. M. *SHELXL-97. A Program for the Refinement of Crystal Structures*; Universität Göttingen: Göttingen, Germany, 1997.